2009

# PREPARATION AND CHARACTERIZATION OF STABLE MACROPOROUS TITANIA NANO-WELLS

Hema Santhi Aluri
*Virginia Commonwealth University*

College of Humanities and Sciences
Virginia Commonwealth University

This is to certify that the thesis prepared by Hema Santhi Aluri entitled PREPARATION AND CHARACTERIZATION OF STABLE MACROPOROUS TITANIA NANO-WELLS has been approved by her committee as satisfactory completion of the thesis requirement for the degree of Master of Science

Dr. Maryanne M Collinson, Director of Thesis, Department of Chemistry

Dr. Sarah C Rutan, Department of Chemistry

Dr. Suzanne M Ruder, Department of Chemistry

Dr. Jason P Rife, Department of Physiology and Biophysics

Dr. Scott Gronert, Chairman, Department of Chemistry

Dr. Fred M Hawkridge, Interim Dean, College of Humanities and Sciences

Dr. F. Douglas Boudinot, Dean of the Graduate School

Date

# PREPARATION AND CHARACTERIZATION OF STABLE MACROPOROUS TITANIA NANO-WELLS

A thesis submitted in partial fulfillment of the requirements for the degree of Master of Science at Virginia Commonwealth University.

by

HEMA SANTHI ALURI
B Pharmacy, Andhra University, INDIA, 2005

Director: MARYANNE M. COLLINSON
PROFESSOR, DEPARTMENT OF CHEMISTRY

Virginia Commonwealth University
Richmond, Virginia
December 2009

## Table of Contents

Page

# List of Tables

Page

# List of Figures

Page

# List of Abbreviations

| | |
|---|---|
| ACAC | Acetylacetone |
| AFM | Atomic force microscopy |
| Ag | Silver |
| AgCl | Silver chloride |
| ALD | Atomic layer deposition |
| $CHCl_3$ | Chloroform |
| CV | Cyclic voltammetry |
| CVD | Chemical vapor deposition |
| DEA | Di-ethanolamine |
| EDS | Energy dispersive X-ray spectroscopy |
| $FcCH_2OH$ | Ferrocene methanol |
| $Fe(CN_6)^{3-}$ | Ferricyanide ion |
| G-SSG | Gas- phase surface sol-gel process |
| HCl | Hydrochloric acid |
| $H_2O$ | Water |
| ITO | Indium tin oxide |
| KCl | Potassium chloride |
| NADH | β- Nicotinamide adenine dinucleotide |

| | |
|---|---|
| ORMOSILS | Organically modified silica |
| PANI | Polyaniline |
| PS | Polystyrene |
| PZC | Point of zero charge |
| RH | Relative humidity |
| $[Ru(bypy)_3]^{2+}$ | Ruthenium tris bypyridyl ion |
| SEM | Scanning electron microscopy |
| $SiO_2$ | Silica |
| SPM | Scanning probe microscopy |
| TMOS | Tetramethoxysilane |
| $TiO_2$ | Titania |
| UME | Ultramicroelectrode |
| XPS | X-ray photoelectron spectroscopy |

# Abstract

PREPARATION AND CHARACTERIZATION OF STABLE MACROPOROUS

TITANIA NANO-WELLS

By Hema Santhi Aluri, M.S.

A thesis submitted in partial fulfillment of the requirements for the degree of Master of Science at Virginia Commonwealth University.

Virginia Commonwealth University, 2009

Major Director: Dr. Maryanne M Collinson, Professor, Department of Chemistry.

Silica based sol-gel thin films have been extensively studied because of their advantages that include optical transparency, high biodegradability and low intrinsic fluorescence.[1] However, one concern with silica based sol-gel derived materials is their long term stability in aqueous solutions.[2-4] Another concern is their limited porosity. These two concerns limit the application of these materials in catalysis and separations.

The main objective of this study is to prepare porous, thin films using titanium alkoxides as precursors and evaluate their long term stability in aqueous solutions. Colloidal crystal templating will be used to introduce macrosized pores into the titania

network. The materials will be characterized using SEM and AFM. To prove that the templated films provide access to the underlying surface of the electrode, a conducting metal like copper was electrodeposited inside the nano-wells. The stability of titania and silica films will be evaluated over a two month period using cyclic voltammetry with three redox probes.

# CHAPTER 1 Introduction

**1.1 Sol-Gel Processing:** The sol-gel process is a versatile solution process for synthesizing a large variety of glass and ceramic oxide materials involving metals like Al, Zn, Si, Ti etc.[5, 6] In general, conventional sol-gel synthesis for preparing inorganic materials involves hydrolysis of inorganic precursor molecules like metal salts or metal organic compounds (e.g. metal alkoxides). When mixed with an organic solvent and water, the metal precursor forms a sol (colloidal particles in solution), which after condensation and polymerization results in an interconnected network between colloidal particles. Subsequent aging and drying results in the evaporation of water and organic solvent from the sol forming a solid skeleton enclosing the liquid phase (gel).[5] For example, silica hydrolyzes and condenses as shown in the following reactions.[2, 5, 6]

Hydrolysis $Si(OR)_4 + nH_2O \rightarrow Si(OR)_{4-n}(OH)_n + nROH$

Condensation: when $n$ =1;

$(OR)_3Si\text{-}OH + HO\text{-}Si(OR)_3 \rightarrow (OR)_3Si\text{-}O\text{-}Si(OR)_3 + H_2O$ (water condensation)

$Si(OR)_4 + HO\text{-}Si(OR)_3 \rightarrow (OR)_3Si\text{-}O\text{-}Si(OR)_3 + ROH$ (alcohol condensation)

An overview of the sol-gel process is represented in Figure 1. Various factors that affect this process include pH, temperature, time of reaction, reagent concentration, catalyst nature and concentration, aging temperature and time, $H_2O$/precursor molar ratio

and drying conditions. By controlling one or a combination of these parameters, ceramic materials with different properties (thickness, surface area, pore size and distribution etc.) can be fabricated.[5, 6]

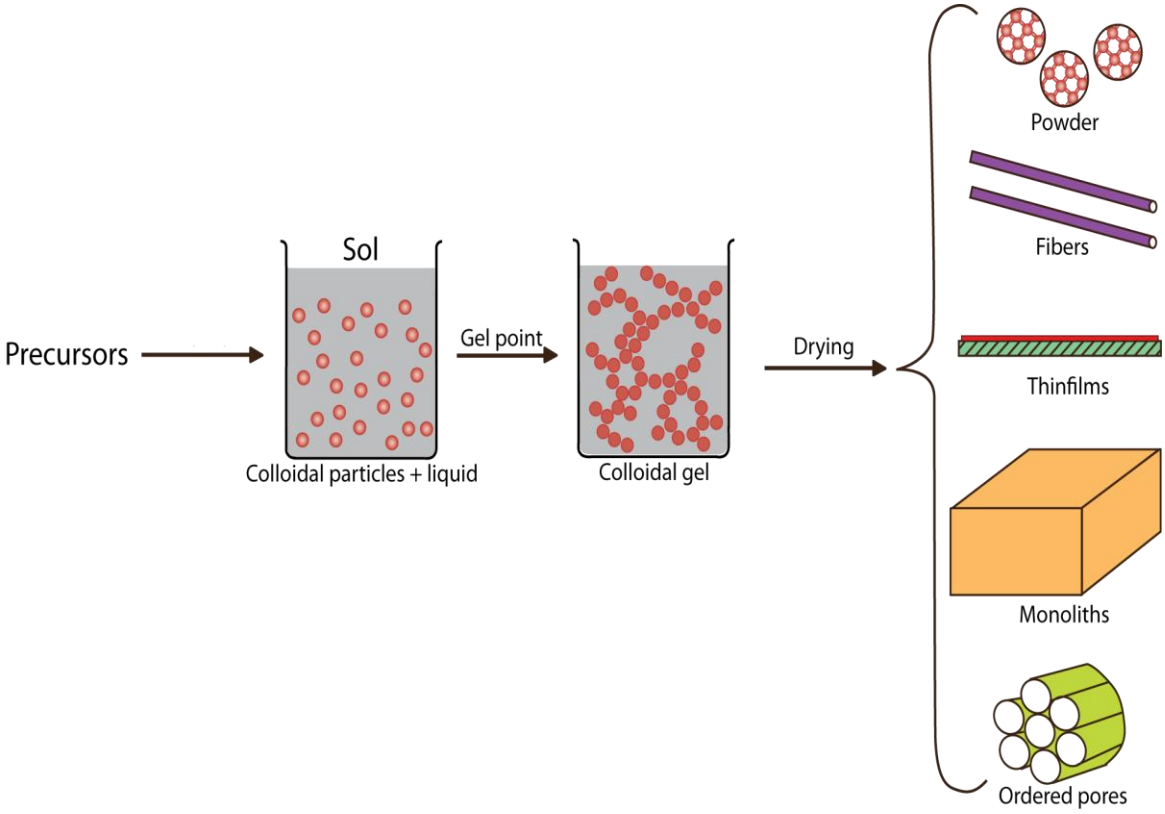


**Figure 1:** Schematic representation of sol-gel process. Adapted from Ref (5).

The sol-gel process is used widely in ceramic or glass industries to fabricate a wide variety of materials ranging from ultra-fine or spherical shaped powders, thin film coatings, ceramic fibers, microporous inorganic membranes, monolithic ceramics and glasses, or extremely porous aerogel materials.[5] Ultra-fine and uniform spherical powders can be prepared by homogenous precipitation, phase transformation or aerosol techniques. Monoliths can be prepared by pouring the sol into a mold, which shrinks upon drying

converting the gel into a dense ceramic. If this drying is done under supercritical conditions, a very low density, highly porous material called an "aerogel" is obtained. Gel fibers drawn from the sol can be converted to glass fibers (application as optical fibers) by adjusting the viscosity and sintering at high temperatures. Thin films can be prepared by spin-coating, dip-coating or electrodepositing the sol on the substrate.[5, 7-10] In spin coating, an excess amount of sol is placed on the substrate and rotated at a high speed. Due to the action of centrifugal force, the sol spreads, forming a thin film on the substrate.[7] Dip coating involves immersing the substrate in the sol and removing it at a specific rate.[7, 11] While spin-coating and dip-coating are the traditional methods used to prepare thin films, electrochemical deposition was recently developed wherein inorganic materials can be deposited on a conducting substrate by applying an electric field.[8-10]

Inorganic-organic hybrid composites can also be prepared which exhibit superior physical-chemical properties like higher mechanical strength, good optical quality, chemical, photochemical and electrochemical stability compared to the materials prepared from simple organic polymers.[1, 12-14] One method by which these materials can be prepared is by physically doping the organic species in the inorganic network.[1, 15, 16] In another method, the inorganic silica framework is synthesized from precursor molecules containing a non-hydrolyzable Si-C bond as shown in Figure 2. Such materials are termed ORMOSILS (organically modified silicas).[12-14, 17] By modifying the organic groups in the precursor molecule, composite materials with different properties like hydrophobicity, porosity, flexibility and stability can be prepared.[12, 13, 18, 19]

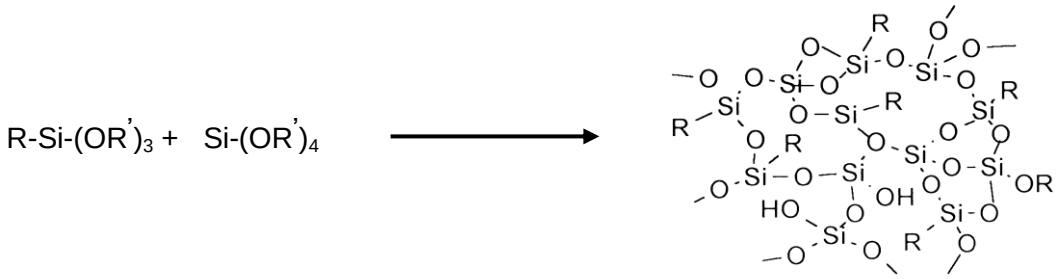


R = $CH_3$, $C_6H_5$, $CH_2CH_2CH_2NH_2$, $CH_2CH_2CH_2SH$

R' = $C_nH_{2n+1}$ (where n = 1, 2, 3,….)

**Figure 2:** Preparation of organically modified silicas (ORMOSILS)

**1.1.1 Applications:** Materials fabricated using the sol-gel process have a wide variety of applications, some of which include membranes for gas and liquid separations, adsorbents, protective coatings, energy storage (e.g. batteries, fuel cells, solar cells), sensors, laboratories on a chip and also in biomedical (micro-pumps, fluid transport systems) devices.[5]

In catalysis, active sites (like metal ions or metal oxides) are incorporated into the inorganic matrix at which catalytic reactions take place.[20, 21] In sensing applications, reagents like chelating agents, proteins, crown ethers, dye molecules, enzymes and antibodies are entrapped into the inorganic matrix and then the external reagent reacts with the entrapped molecule generating a response.[1, 15, 16, 22] So, it is important that the host inorganic matrix be porous enough for the external reagent to diffuse in and then react with

the entrapped molecule.[23] The two most extensively used sol-gel derived configurations for both of these applications are monoliths and thin films. Thin films have an advantage that there is a short path for diffusion of reagents to the substrate surface, thus improving the response times and recovery rates.[13] Sol-gel thin film materials have gained considerable attention in the field of catalysis and sensing.[1, 16, 21, 24-26]

**1.1.2 Advantages and disadvantages of sol-gel process compared to conventional techniques:** Compared to conventional techniques like melting, chemical vapor deposition (CVD) and atomic layer deposition (ALD), sol-gel fabricated materials have improved homogeneity and purity.[5, 6] The low temperature processing minimizes energy consumption, evaporation losses and air pollution. Also, during the preparation of these materials, the interactions between the chemicals and containers, phase separation and crystallization can be avoided.[27] New materials with different chemical compositions (e.g. mixture of metals), configurations (fibers, powders, films etc.) and special properties can be made.[5, 22] Along with the above mentioned advantages, the sol-gel process also provides an efficient way to incorporate heat sensitive materials like organic molecules and proteins into ceramic materials.[15, 28] However, certain disadvantages like expensive raw materials, large shrinkage upon drying, uncontrollable pore morphology, formation of residual hydroxyls when in water (interaction with $OH^-$), health hazards from materials used and time consumption need considerable attention.[27]

**1.2 Templating:** The porosity of thin films prepared by spin coating the sol on a substrate is much less (60-70 %) when compared to monoliths due to the overlap of the gelation/drying phases.[29] By improving the porosity of the films by using templates, these

materials can have wider applications in chemical sensing and separations and also as templates to grow nanostructures inside the nano-wells.[30-33]

The concept of templating has been widely employed to make porous materials. Both the type of porous matrix and the shape and size of the pores have been successfully tuned.[33-35] In general, porosity is defined as the measure of void space in the material. Templated materials can be micro, meso or macroporous depending on the pore size. Materials that have pores with $d < 2$ nm are termed microporous while those with $2 \text{ nm} < d < 50$ nm are called mesoporous materials. Materials with pores having $d > 50$ nm are said to be macroporous. Dickey's paper on preparing porous silica templated with dye is one of the pioneering works in the fabrication of molecular imprinted materials.[36] The first step in the templating (imprinting) process involves incorporating foreign species (template) into the sol, which after condensation and polymerization gets embedded into the polymeric matrix. In the next step, the template is removed leaving a structured impression of the template in the gel matrix, as shown in Figure 3.[35] Examples of such species are emulsion droplets,[37] latex spheres,[33, 38] surfactants,[32, 39-41] dendrimers,[42-45] sugars like D-glucose[46] and even biological materials like bacteria.[47-49] An ideal template should be chemically and thermally stable/robust during the preparation process. Finally, the template should be easily removed leaving the structured impression in the film surface.[50] Templating can be extended to the preparation of various types of materials including alloys,[51, 52] metals and non metals,[53-56] organo-metallic materials,[57] polymers,[58-61] simple oxides[56, 57, 62-65] and ternary oxides.[57, 66]

The concept of fabricating highly ordered porous structures was introduced in early 1950's with the synthesis of zeolites (microporous alumino-silicates). These materials became commercially very successful due to their unique properties like high surface area, crystalline structure, acidity, ion-exchange capacity and selectivity (shape).[67] The diffusion of molecules through these crystalline solids is very limited because their pore size is confined to only a few nanometers (d < 2 nm).[67] In the early 90's, Kresge et. al. and Beck et al. reported the creation of ordered inorganic mesoporous materials using ionic surfactants as templates.[68, 69] In addition to the advantages provided by the sol-gel process, these templated materials offer high surface area and defined porosity.[34, 35] Since then there has been great progress in developing templated porous materials with tunable properties like pore structure, composition, pore size and texture.[33, 39, 57, 70]

**1.2.1 Colloidal crystal templating:** One means to introduce defined macropores into sol-gel derived materials utilizes colloidal crystals as templates. Colloidal crystals are often made from polymer spheres such as polystyrene, poly-(methyl methacrylate), or mono-disperse silica.[33] In this kind of templating, the colloidal spheres are arranged in a close-pack arrangement and then the interstitial spaces are exposed to/filled with the precursor solution (i.e. sol) which, after gelation/drying forms a dense matrix. Removal of the template leaves well ordered pores in the matrix that have similar dimensions of the colloidal crystal.[33, 35, 38] Figure 3 shows a pictorial representation of colloidal crystal templating in inorganic materials. Another approach to fabricate structured materials involves dual templating with colloidal crystals, wherein materials with bimodal porosity can be prepared.[57, 71-73] For example, Wu et. al. used cationic cetyltrimethylammonium

($CTA^+$) micelles and microscale polystyrene (PS) latex as templates to prepare "raspberry-like" inorganic $SiO_2$ hierarchical nanostructures.[74]

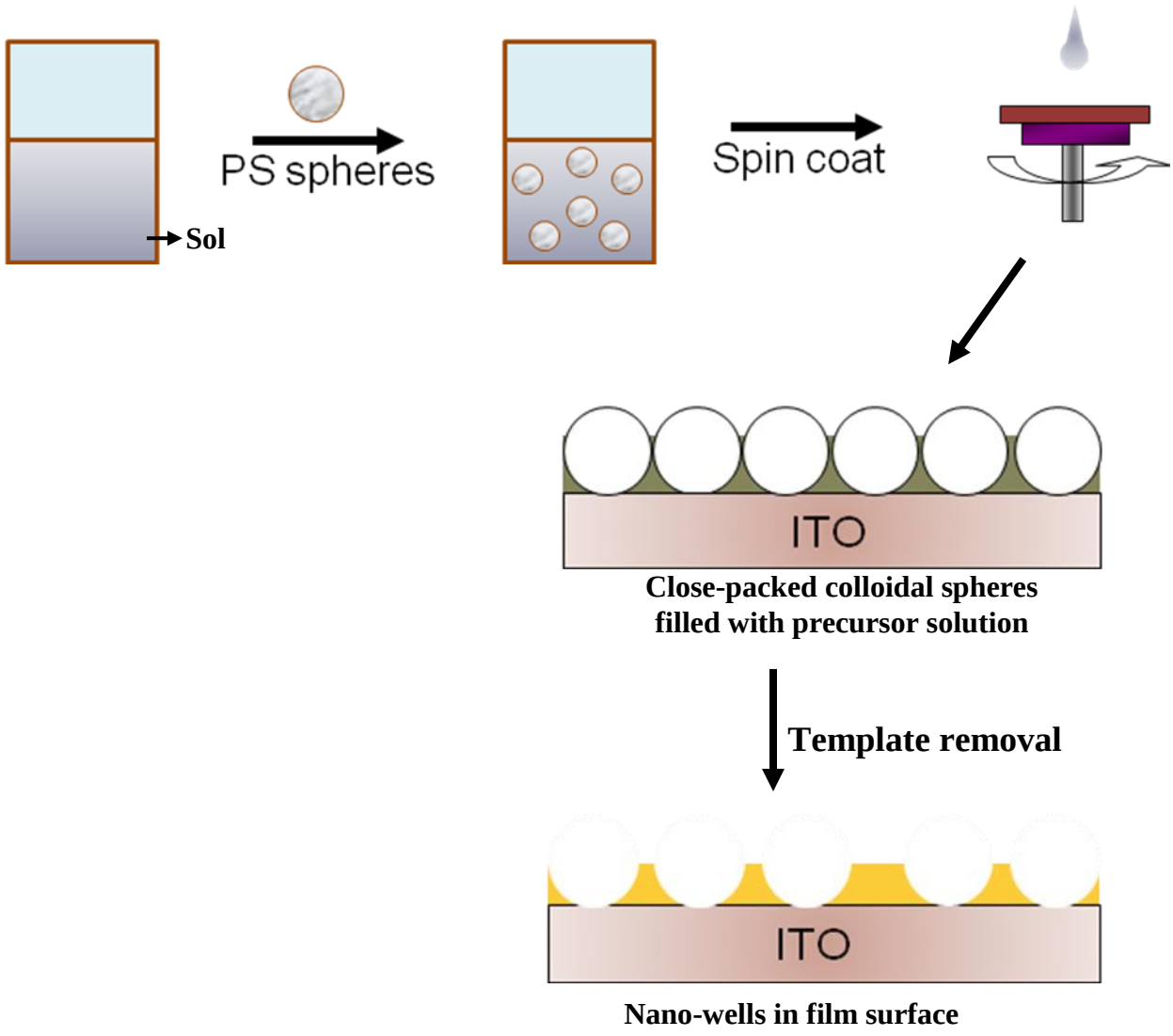


**Figure 3:** Schematic showing colloidal crystal templating in inorganic materials using spin coating.

Colloidal crystals can easily be assembled on the substrate by techniques like dip coating,[11, 75] spin coating[76, 77] and electrophoretic deposition.[78] For the colloidal spheres to assemble into a uniform closely packed monolayer on a substrate surface, it is important for the solution (of colloidal spheres) to wet the substrate surface completely.[38] Electrostatic forces between the surface and spheres are also important.[79] This method of templating can be extended to fabricate materials using techniques other than sol-gel[35, 57, 62-65, 80] like electrochemical (electrodeposition),[81-83] chemical vapor deposition,[84, 85] electroless deposition,[86, 87] spraying,[88, 89] oxide and salt reduction,[52, 56, 90] patterning[91] and inverse opal[92-94] methods.

Many researchers have focused their attention on increasing the surface area of the inorganic materials by templating with colloidal crystals and using these materials in catalysis and sensing devices. In 2001, the Collinson group reported a convenient way of increasing the porosity of silica sol-gel derived materials using PS spheres.[95] Later, the Collinson group fabricated macroporous silica sol-gel materials by forming a single continuous layer of PS spheres and finally removing the PS by a mild chemical treatment. Copper and polyaniline (PANI) were electrodeposited into the nano-wells to prove that nanostructures can be grown inside the nano-wells.[76] Levy et al. showed that the templated inorganic materials can be used to make ion-exchange columns for use in chromatographic instruments. In this work, a quaternary ammonium salt called cetylpyridinium is trapped into a solid silica support and the columns produced from this are found to be particularly useful in the analysis of $Cl^-$, $Br^-$ and $SO_4^{-2}$.[96] Tian et al. showed that when compared to the unpatterned films, PANI composite templated films showed a higher electrocatalytic

efficiency for oxidation of reduced β-nicotinamide adenine dinucleotide (NADH).[97] Also, Song and co-workers showed that the templated films with platinum nano-particles showed a much more efficient detection of glucose compared to directly deposited platinum.[98] From the research cited above, it is clear that as a result of the large surface area of the templated films, they exhibit higher efficiency compared to ordinary modified electrodes.

Though sol-gel derived templated silica thin films have become very popular, one of the major drawbacks is that these films form surface hydroxyls on the film surface over a period of time in aqueous solutions.[2, 99, 100] It has been experimentally shown by the Collinson group that as the silica films sit in water for 46 hrs, defects develop in the film, eventually resulting in the film falling off from the substrate.[101] This can be attributed to the hydroxyl (Si-OH) formation that results in breaking of the polymeric gel structure, which could lead to decreased material performance and increased solution contamination. Research to improve the hydrolytic stability of mesoporous silica materials has led to the fabrication of alternate materials. Materials with various physicochemical properties were prepared by introducing various organic functional groups into the inorganic alkoxide precursor which then form organically modified silicas (ORMOSILS).[12-14] Another way to improve stability is to add secondary metal oxides of Al,[100, 102-106] Ti,[107, 108] and La[109] to pure silica materials during or after synthesis. However, both the above mentioned materials suffer from the disadvantages originating from siloxane backbones. As an alternative, pure inorganic materials derived from transition metal precursors by sol-gel process were thought to improve the stability to a very large extent.[110, 111] The dissolution of the films in aqueous solutions is mainly dictated by the charge of the metal oxide in the

films, which show minimum solubility around its point of zero charge.[112, 113] Using this concept, the preparation and characterization of stable macroporous materials using one such transition metal (titanium) has been investigated and is presented herein.

**1.3 Titanium sol-gel chemistry:** $TiO_2$ films can be synthesized using sol–gel processing through the hydrolysis and condensation of corresponding alkoxides of the general formula $Ti(OR)_n$, where R is an alkyl group.[114] The first step in this process is the hydrolysis of the titanium precursor, which upon further water and alcohol condensation forms -Ti-O-Ti- bonds as shown in the reactions below. Further, a series of condensation reactions result in the linking of additional –Ti-OH that eventually results in the formation of $TiO_2$ network.[5, 114]

Hydrolysis: The hydrolysis takes place in an alcohol medium with the addition of water.

$$Ti(OR)_4 + nH_2O \longrightarrow Ti(OR)_{4-n}(OH)_n + nROH$$

Condensation: when n= 1;

$$Ti(OR)_3(OH) + Ti(OR)_3(OH) \longrightarrow (RO)_3Ti\text{-}O\text{-}Ti(OR)_3 + H_2O \text{ (water condensation)}$$

$$Ti(OR)_3(OH) + Ti(OR)_4 \longrightarrow (RO)_3Ti\text{-}O\text{-}Ti(OR)_3 + ROH \text{ (alcohol condensation)}$$

Both the hydrolysis and condensation reactions occur via a $S_N2$ mechanism. In a basic environment, hydrolysis involves a nuclephilic attack on the metal atom by a hydroxide ion followed by the displacement of an alkoxide ion whereas under acidic conditions, protonation of the alkoxide group occurs followed by the nucleophilic attack of water resulting in the formation of titanium intermediates.[5]

However, titanium alkoxides are more challenging to work with, compared to silicon alkoxides because they hydrolyze very fast when exposed to $H_2O$. This is explained by the higher electrophilic nature of titanium and it ability to increase its coordination number. Hence, titanium alkoxide precursors (e.g. Titanium n-butoxide) are complexed with agents like acetylacetone (ACAC) or diethanolamine (DEA) to decrease the rate of hydrolysis as shown by the following reactions:[114, 115]

$$Ti(OBu^n)_4 + acacH \longrightarrow Ti(OBu^n)_3(acac) + BuOH$$

$$Ti(OBu^n)_4 + HN(C_2H_4OH)_2 \longrightarrow Ti(OBu^n)_3[HN(C_2H_4O)_2] + BuOH$$

Both acetylacetone and diethanolamine when added in a one to one molar ratio acts like a bidentate chelating agent forming an intermediate complex which is five coordinated. Acetylacetone forms a complex by chelation between its carbonyl oxygens and titanium metal center. When diethanolamine is used as a stabilizing agent, the intermediate complex is formed by chelation of its hydroxyl groups with the titanium metal center. Condensation takes place with the addition of water whereby the less electronegative groups (e.g. alkoxy groups) are easily and quickly replaced (by $OH^-$) when compared to the more electronegative groups (acac, diethanolamine). Hence, the strongly bonded acac and amine groups in the above reactions are very difficult to hydrolyze when compared to the butoxy groups. This decreases the rate of hydrolysis of the intermediate complexed precursor and eventually condensation to form $TiO_2$.[114, 116]

The titanium alkoxide precursor used in our study is titanium *n*-butoxide. The precursor is complexed with diethanolamine and the hydrolysis is initiated by adding

ethanol and water to the mixture. The sol is stirred for few hours and is left to age in a desiccator for two days.

Colloidal crystal templating has also been done in materials prepared using a titanium based precursor[117, 118] because of its advantages like high thermal and aqueous stability, which can be important in applications like electrochemical sensing, catalysis and electronic devices. Many research groups have used the vertical deposition method to first assemble spheres on the substrate and then immerse the substrate into a titania sol. The voids between spheres were filled with the sol which after drying and calcination to remove PS spheres forms replicas in the $TiO_2$ films.[119, 120] A modified method was proposed by Li et al. in which mechanically robust $TiO_2$ films were prepared by a gas-phase surface sol-gel process (G-SSG), in which the pre-casted spheres on the glass substrate were exposed to titania vapor which condenses on top of the spheres to form a nm layer film.[121] Until presently, most of the work done involved preparation and characterization of multilayered (3-D) or monolayer (2-D) templated titania films. Though the literature suggests that materials prepared from transition metals (e.g. titania, zirconium) have higher stability,[110, 111] it is important to study and prove the hydrothermal stability of these films in water or any electrolyte solutions, which is one of the main objectives of the experimental study.

In this work, a combination of transition metal oxide (titanium) as a precursor and colloidal crystal templating was employed to prepare macroporous thin films. First, a well-packed monolayer of PS spheres in the titania matrix was undertaken. Second, the PS spheres were removed completely leaving bowl-shaped replicas in the film. Third, the

stability of the titania films in aqueous media (0.1 M KCl) was studied for a period of two months and compared to conventional silica templated films.

**1.4 Motivation:** The main motivation of this work was to prepare better materials for applications like chemical or biological sensing. An ideal sensor should have the following properties: faster response times, good recovery rate and higher sensitivity. In addition, these sensors should exhibit long term stability and recyclability to be commercially successful.[28, 122, 123]

In general, a dopant (i.e. receptor) is embedded in the sol-gel derived inorganic matrix and interacts with the analyte molecule in solution to generate a measurable response.[15] Commonly used dopants include indicator dye molecules, chelating agents, biomolecules (enzymes, antibodies, and other proteins), crown ethers, and metal particles.[15, 20, 124, 125] The response generated results from one of the following chemical reactions between the dopant and the analyte molecule: proton-transfer and redox reaction, complexation, ligand exchange or an enzymatic reaction.[15] There have been numerous advances in preparing sensors using the sol-gel technique because the materials prepared from this process are chemically inert, have good optical transparency, higher surface area and porosity. Also, the dopant can be easily incorporated into the matrix since the initial steps in this process are in the liquid phase. Furthermore, since the process is carried out at ambient temperature conditions, even biomolecules like enzymes or proteins can be easily entrapped into the sol-gel matrix.[15, 28, 122, 123, 126-128]

Among the different material configurations prepared using sol-gel process, thin films have gathered considerable attention because of their shorter path for diffusion of the

analyte through the film to react with the dopant or to reach the substrate surface. However, the porosity of thin films prepared by spin coating the sol on the substrate is much less (60-70 %) when compared to monoliths due to the overlap of the gelation/drying phases.[29] Hence, it is important to increase the porosity of the thin films (by templating) because this feature allows for analyte molecule in solution to more quickly reach and react with the dopant. Also, the templated materials provide greater surface area (see Figure 4) compared to bulk materials. Both these features (porosity and high surface area) improves the response time and recovery rate of the sensor material.[13, 30-33]

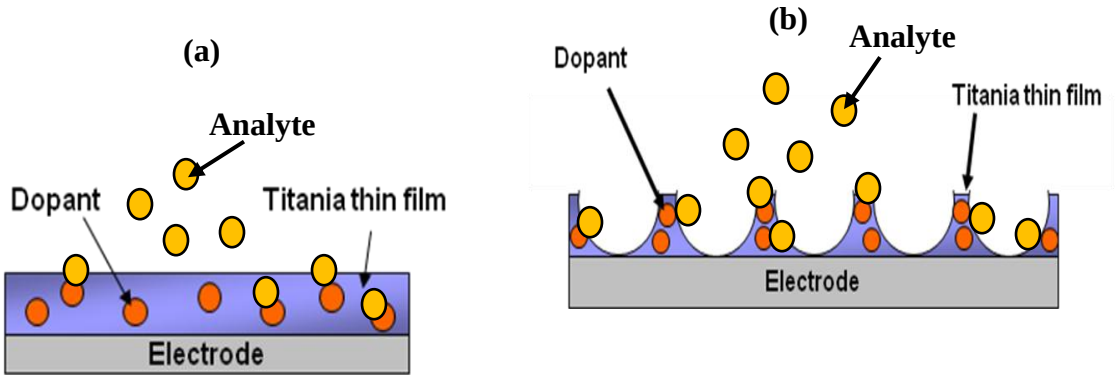


**Figure 4:** Pictorial representation of a dopant embedded in a (a) titania thin film (b) templated titania film and its reaction with an analyte in solution.

One important drawback that needs to be addressed is the loss of the dopant that is embedded in the film when placed in aqueous solutions.[123] This decreases the sensor performance, reduces recyclability and increases the solution contamination. One of the major reasons for this can be attributed to the disruption in gel structure of the films (e.g. silica film) when placed in aqueous solutions as shown in Figure 5. Hence it is important

that the films are stable when they are kept in aqueous solutions for a few days to months. A solution for this problem is to prepare thin films that are stable in aqueous media for longer periods. The hypothesis that forms the basis of this work is that titania sol-gel templated films will not only have controlled macroporosity and higher surface area but will also be more stable in aqueous solutions.

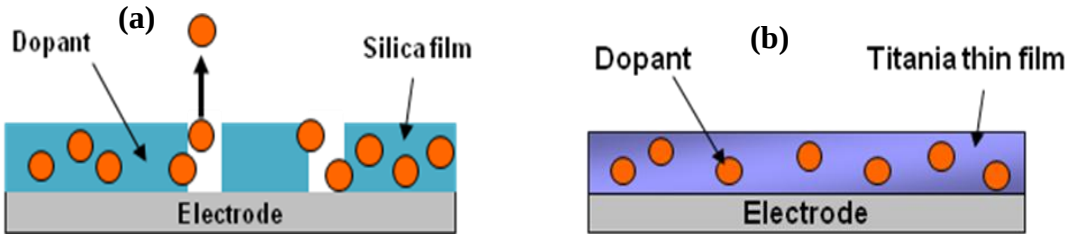


**Figure 5:** Pictorial representation of a dopant embedded in a (a) silica thin film (b) titania thin film.

# CHAPTER 2 Methods and Materials

The preliminary studies on the preparation of monolayer packed templated titania thin films and their characterization using AFM (Atomic Force Microscopy), SEM (Scanning Electron Microscopy) and CV (Cyclic Voltammetry) are presented here. Stability tests are also presented to verify the stability of $TiO_2$ films compared to the more conventionally used silica thin films.

**2.1 Reagents and equipment:** Titanium (IV) *n*-butoxide (99 %), tetramethoxysilane (TMOS, 99 %), ferrocene-methanol ($FcCH_2OH$, 97 %) were purchased from ACROS Organics. Diethanolamine (DEA), chloroform, cupric sulfate, sulfuric acid, potassium chloride and 1-butanol were purchased from Fisher Scientific. Octyltrimethoxysilane (octyl-TMOS, 96 %), tris (2, 2'- bipyridyl) dichlororuthenium (II) hexahydrate ($[Ru(bypy)_3]\ Cl_2.\ 6H_2O$, 99.95 %), potassium ferricyanide (III) ($K_3Fe(CN)_6$, 99 %) were purchased from Aldrich. Acetylacetone (ACAC) was purchased from FLUKA. 200 proof-absolute, anhydrous ethyl alcohol was purchased from PHARMCO- AAPER. Aqueous suspensions of polystyrene microspheres (PS) with a diameter of 0.47 μm were purchased from Invitrogen molecular probes (8 % w/v, sulfate latex). Water was purified to distilled

water using Milli-Q (Millipore) four-cartridge system. The ITO (indium tin oxide coated on glass) slides were purchased from Delta Technologies LTD.

AFM was performed with a Veeco Multimode$^{TM}$ (version 5) scanning probe microscope (SPM) used in a tapping mode with high aspect ratio tips (Vista probes from Nanoscience instruments) at scan rates varying between 0.2-1 Hz. SEM images were obtained from Zeiss EVO 50 XVP scanning electron microscope. Prior to imaging, the samples were sputter coated with a thin layer of gold using an EMS 550X sputter coater to avoid charging effects. Electrochemical experiments were carried out using a CH instruments potentiostat. The cell consists of a single chamber with three electrodes wherein the reference and auxiliary electrodes were an Ag/AgCl (1 M KCl) and platinum wire respectively, and the working electrode was ITO coated on glass.

**2.2 Procedure:** A monolayer of closely arranged spheres can be formed on the substrate by mixing latex spheres with sol and spin casting it on the substrate.[129] Early work on preparing a stable titania sol was started by using ACAC as the complexing agent. In this recipe, 0.2 g of titanium *n*-butoxide, 0.5 mL butanol, 50 µL ACAC and 100 µL $H_2O$ were added in that order with continuous stirring and left aside in the desiccator for one day. The resulting titania sol was mixed with latex spheres and spun on a glass substrate. Visual observation by eye showed randomly distributed black particles in the sol mixture. AFM images of such samples showed areas with multi-layers of polystyrene spheres and some areas without any packing (see chapter 3). Various parameters like pH, complexing agent and cleaning of the substrate were considered in the preparation of well-packed titania

films. AFM and SEM imaging were done to characterize the titania films which provided more details about the effect of each parameter in synthesizing ordered materials.

**2.2.1 Cleaning the Substrate:** ITO / glass slides were cut into uniform pieces (1.5 cm x 1.5 cm), washed in methanol 2-3 times followed by water 2-3 times and then soaked in soap solution for one day to impart a negative charge on the surface. Prior to casting the film on the substrate the slides were thoroughly rinsed several times leaving a clean, negatively charged surface.

**2.2.2 Preparation of films:** Titania sols were prepared by adding 0.3 g of diethanolamine (DEA) to 0.3 g of titanium *n*-butoxide under continuous stirring. Then 0.6 g of ethanol was added to the complexed titanium mixture and stirred for 2 h. After 2 h, 0.2 mL of $H_2O$ was added and the stirring was continued for 2 h. Silica sols were prepared by stirring a mixture of 0.25 mL TMOS with 1.2 mL methanol, 1.15 mL $H_2O$ and 0.15 mL 0.1 M HCl for 30 min. Both sols were left in a desiccator for two days before spinning on soap cleaned ITO slides. Before spinning, the polystyrene latex spheres were sonicated for 5-10 min and then mixed with either a titanium sol in a 2:1 (sphere: sol; v/v) ratio or a silica sol in a 3:2 (sphere: sol; v/v) ratio. The sol doped with PS spheres was then spin-cast on ITO (approx. 20 µL) using a G3-8 spin coater (from Cookson Electronics) at 2500 rpm for 25 sec. The coated samples were dried at a constant temperature ($30^oC$- $35^oC$) and humidity (approx. 35- 40 %) for two days in an Isotemp Oven (from Fisher Scientific).

**2.3 Blocking the defects in silica and titania films:** After spin-casting, the films prepared from both the sols contain defects that need to be blocked. For films prepared from the titania sol, the defects were blocked by casting (2500 rpm, 25 sec) a dilute titania sol using

ACAC as complexing agent. This sol made for blocking was prepared by complexing 0.2 g of titanium *n*-butoxide with 20 µL ACAC and 3 mL butanol followed by continuously stirring for 2 h. For silica films blocking was done by soaking the films in a dilute solution of octyl-TMOS (7.5 % w/v in dry ethanol) for 4 h followed by rinsing with ethanol (4- 5 times). Both titania and silica films were dried at a constant temperature ($30^oC$ - $35^oC$) and humidity (approx. 35- 40 %) for two days in an Isotemp Oven (from Fisher Scientific).

After drying, the titania films were calcined in a Thermolyne (type 1500) muffle furnace to remove the polystyrene spheres by increasing the temperature from $25^oC$ to $435^oC$ at a ramp of $3^oC$. The temperature was then held at $435^oC$ for 25 min followed by cooling back to $25^oC$. The calcined films were thoroughly rinsed with distilled water to remove any residual carbon on the films. For silica films, the PS spheres were removed by soaking in chloroform for one hour and then rinsed them 4-5 times with ethanol. Figure 6 shows a cartoon of the steps carried in the preparation of templated porous titania and silica films.

**2.4 Stability experiments:** Figure 7 gives a pictorial representation of the three electrode electrochemical cell used to collect the CV's. Three different redox probes with different charges were chosen to evaluate the stability of the films by measuring the current flow through the films. They were (1) tris (2, 2'- bipyridyl) dichlororuthenium (II) hexahydrate [114], (2) potassium ferricyanide (III) [$K_3Fe(CN)_6$- negative], (3) ferrocene-methanol [$FcCH_2OH$- neutral]. Stability studies were performed for samples soaked in 0.1 M KCl for a period up to two months for titania films and one week for silica films. The electrode area was approximately 2.0 $cm^2$. A piece of copper tape was attached to each ITO

electrode (sample) and the samples were soaked in 0.1 M KCl solution. The samples were

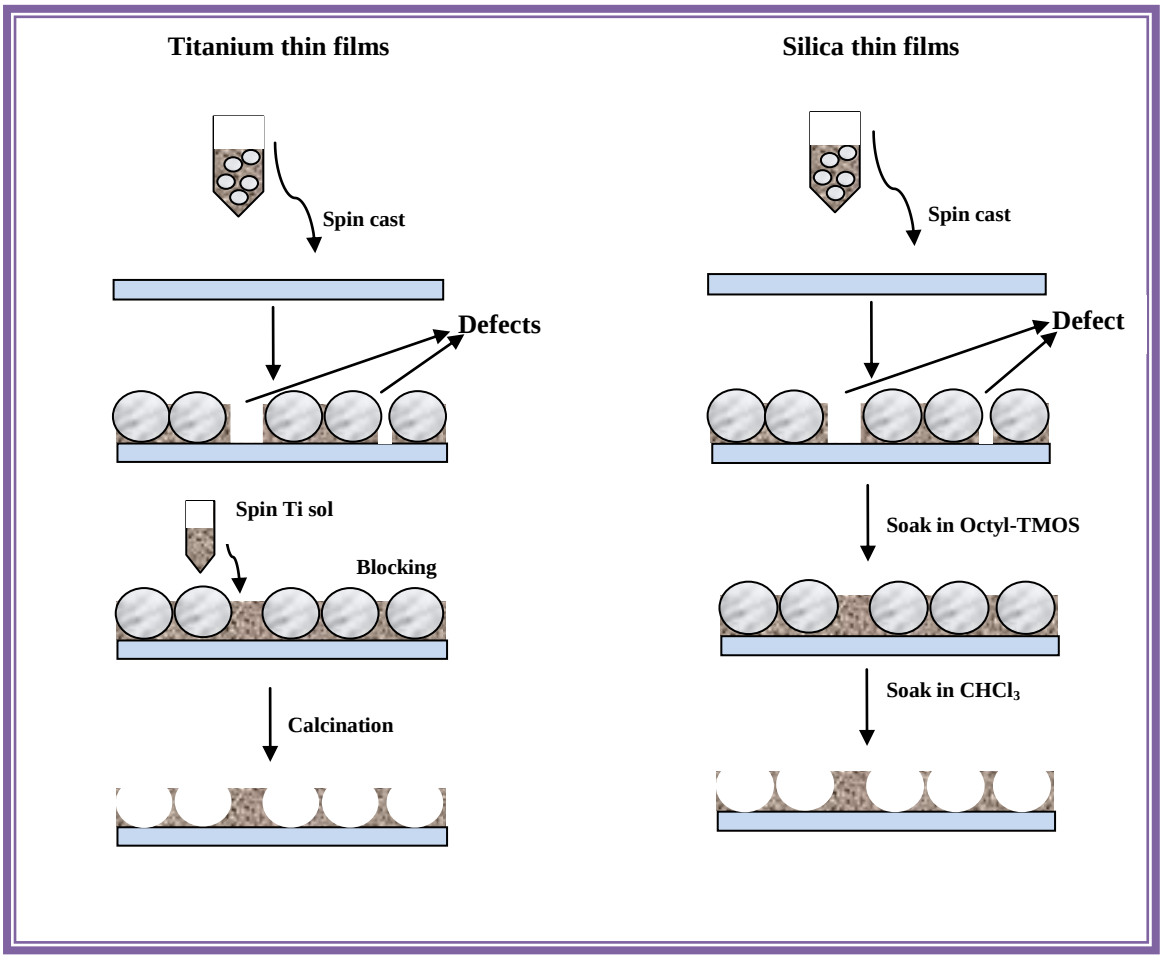


**Figure 6:** Schematic cartoon for titania and silica film preparation containing nano-wells. Not drawn to scale.

periodically taken out of the KCl solution and washed 2-3 times to remove any residual KCl on the films. The CV's were then collected in a redox probe solution (1 mM in 0.1 M KCl) as shown in Figure 7. While collecting the CV's, in order to minimize the movement of the electrode in the solution, the electrode was made more rigid by sandwiching the copper tape between two glass slides (see Figure 7). After collecting the CV's, the samples

were washed 2-3 times with water to remove any adsorbed redox probe on the surface and were finally transferred to the 0.1 M KCl solution. The only problem with this configuration was that the areas of the electrode immersed in the probe solution vary each time and with different samples. Since the current measured depends on area, this created problems when comparing CV results from two different electrodes.

AFM images were collected on titania samples taken from 0.1 M KCl after 15, 30 and 60 days whereas for silica films, the images were taken after the 3$^{rd}$ and 5$^{th}$ day. These images were used to study any variations in surface morphology of the films.

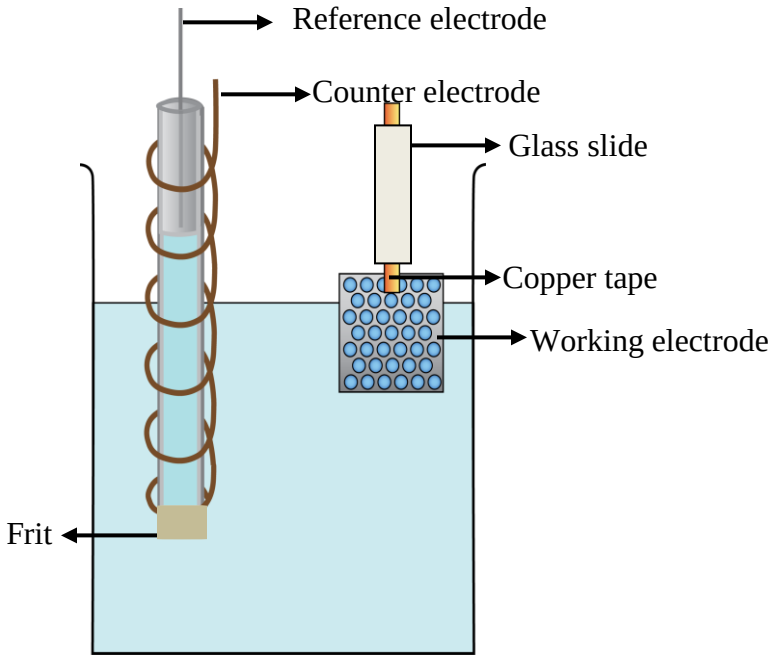


**Figure 7:** Cartoon showing the electrochemical cell that contains a Ag/AgCl (1 M KCl) reference electrode and a platinum wire as the counter electrode. The ITO working electrode was immersed in the solution by attaching it with a copper tape. Not drawn to scale.

# CHAPTER 3 Results and Discussion

Macroporous titania thin films were prepared after the template, physically entrapped in the sol,[76, 77, 129] was removed after spin-coating on a clean substrate which leaves its impression in the $TiO_2$ matrix. The macroporosity of the films can be tuned by controlling the size and shape of the template. An ideal template should be available in various sizes and/or shapes and easily removed leaving its "imprint" in the host structure.[35] PS spheres have all these properties and therefore were an ideal template to fabricate macroporous inorganic structures.

In this experimental study, an ordered layer of PS spheres in a titania film was first formed. In the next step, the spheres were removed either by chemical or heat methods. After the spheres were removed, electrochemical experiments were performed to verify that no residual material remained in the bottom of the nano-wells. The stability of the titania films was evaluated and compared to silica films by soaking in aqueous 0.1 M KCl for a set period of time. These stable titania nano-wells were then used as templates to grow copper inside them.

**3.1 Preparation of ordered monolayer of PS spheres in $TiO_2$ matrix:** Some of the important factors that play a role in preparation of close-packed array of PS spheres in titania films include the pH of the sol, complexing agent, cleaning of the substrate, sol-to-

sphere ratio and precursor-to-complexing agent ratio. Titanium materials prepared from titanium *n*-butoxide often use acetylacetone as a complexing agent to slow the rate of hydrolysis.[130, 131] However, when these traditional procedures were used in these experiments, the PS spheres formed several layers/clumps in the titania matrix as shown in Figure 8. One problem with this recipe was that the pH of the titania sol was less than the isoelectric pH of titanium which is 6.2.[132] Colloidal sols of titanium above this point have a net negative charge and at a lower pH have a net positive charge. To form a monolayer of spheres on the surface, it is important that the charge on the latex sphere and the surface be the same.[38] When the surface and the PS spheres have opposite charges, the PS spheres are forced to arrange on the surface that results in forming clumps or several layers in the film surface. However, the same charge on the PS spheres and the surface allow free movement of the PS spheres on the substrate surface to take place due to repulsive forces between them that helps in forming an ordered packed monolayer. In the experiments performed, since the charge of the PS spheres used was negative, a negative charge on the surface was needed to help achieve an ordered array of PS spheres. So, a basic complexing agent like diethanolamine (DEA) was used to increase the sol pH giving a stable sol with a net negative charge assisting in the formation of well-packed monolayers.

After a number of trials, a procedure to reproducibly fabricate templated porous titania films was determined. Though various compositions and combinations have been tried with the diethanolamine complexing agent, in most cases, the spheres arranged themselves in a hexagonally close packed array. The effect of the various parameters on packing of the PS spheres in the $TiO_2$ matrix was evaluated from images taken using AFM.

Some of these varied parameters that showed an improvement in the preparation procedure are listed in Table 1.

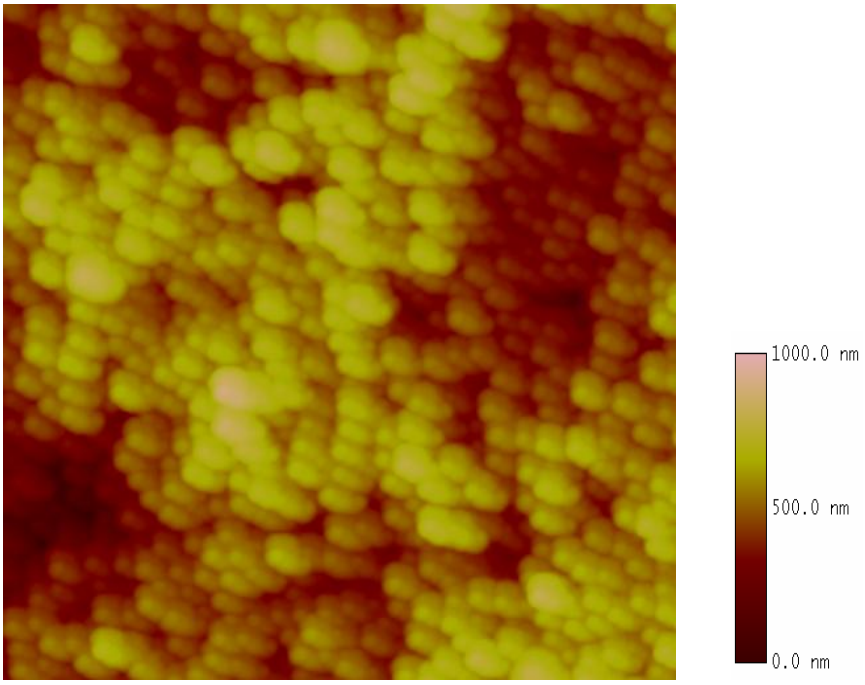


**Figure 8:** A 15 µm x 15 µm AFM image of $TiO_2$ films with PS spheres prepared from using the recipe: 0.2 g of titanium *n*-butoxide, 0.5 mL butanol, 50 µL ACAC and 100 µL $H_2O$. Image shows several layers of PS spheres in the $TiO_2$ matrix.

**Table 1:** Different procedures used to prepare titania sols for achieving a well-packed monolayer and the observations made visually by eye or from images obtained using AFM.

| Procedure | Varied parameter | Observation(Visual/AFM) |
|---|---|---|
| 0.2 g Ti + 0.5 mL butanol + 50 µL ACAC + 0.1 mL $H_2O$. Substrate cleaned with water and ethanol. Sol:PS sphere ratio- 1:1 | | Visual: Black particles in the sol.<br>AFM: Uneven distribution of multilayered PS spheres. |

| | | |
|---|---|---|
| 0.9 g Ti + 0.23 mL 6M HCl + 1.2 mL ethanol + 0.75 mL $H_2O$. Substrate cleaned with water and ethanol. Sol:PS sphere ratio- 1:1 | Complexing agent, pH: 2.0-2.5, solvent | AFM: Several layers of PS spheres. |
| 0.9 g Ti + 1.5 mL acetic acid + 1.5 mL ethanol: stir for 15 min. Substrate cleaned with water and ethanol. Sol:PS sphere ratio- 1:1 | Complexing agent, pH: 3.0-3.5 | Visual: Sol gelled. |
| 0.7 g Ti + 0.6 mL acetic acid (12M) + 0.3 mL ethanol + 0.15 mL $NH_3$ (1M). Substrate cleaned with water and ethanol. Sol:PS sphere ratio- 1:1 | Complexing agent, pH: 5.0-6.0 | AFM: Better packing with some multilayer formation. |
| 0.7 g Ti + 0.6 mL acetic acid (12M) + 0.3 mL ethanol + 0.15 mL $NH_3$ (1M). Sol:PS sphere ratio- 1:1 | Cleaning of the substrate: plasma cleaned | AFM: No uniform packing. |
| 0.7 g Ti + 0.6 mL acetic acid (12M) + 0.3 mL ethanol + 0.15 mL $NH_3$ (1M). Sol:PS sphere ratio- 1:1 | Cleaning of the substrate: soap cleaned | AFM: Better packing compared to plasma cleaned samples. |
| 0.7 g Ti + 0.6 mL acetic acid (12M) + 0.3 mL ethanol + 0.15 mL $NH_3$ (1M). Soap cleaned substrate. | Varying sol:PS sphere ratio – 1:1.5 | AFM: Improved packing with little white areas not packed uniformly. |

| | | |
|---|---|---|
| 0.6 g Ti + 0.3 g di-ethanolamine + 0.6 mL ethanol + 0.2 mL $H_2O$. Soap cleaned substrate. Sol:PS sphere ratio- 1:1.5 | Complexing agent, pH: 6.0-7.0 | AFM: Monolayer packed films with better distribution on the substrate. |
| 0.3 g Ti + 0.3 g di-ethanolamine + 0.6 mL ethanol + 0.2 mL $H_2O$. Soap cleaned substrate. Sol:PS sphere ratio- 1:1.5 | Ratio of precursor to complexing agent, pH: 6.0-7.0 | AFM: Monolayer packed films with improved distribution on the substrate when compared to the earlier one. |

Three different microscopic methods were used to evaluate how the spheres pack in the titania film coated on ITO: optical, AFM and SEM. Optical microscopy provides a cursory view of the surface as it is limited to the resolution of an optical microscope. SEM and tapping mode AFM are high resolution imaging techniques that reveal microscopic details of the sample surface. While AFM allows images to be acquired under room conditions, SEM is operated under vacuum conditions. In SEM, the electrons from the high energy electron beam interact with the atoms on the sample surface generating a signal which gives information on surface topography and in some cases composition. This type of imaging is quick for studying morphology for large areas of the sample. Figure 9 shows a 30 µm x 30 µm SEM image of 2-D ordered monolayer of latex spheres. Slight disorders in the packing are seen, likely due to the imperfections and scratches from the cutting or cleaning of the ITO.[76] Typically, the AFM utilizes a micro-cantilever with a sharp tip to scan the sample surface. In a tapping mode AFM, the Van der Waals forces

existing between the tip and the surface decrease the resonance frequency of the cantilever which is maintained by the feedback loop system by adjusting the average tip-to-sample distance. By measuring the tip-to-sample distance at each (x, y) data point, the topographic image of the sample surface can be obtained. The insets in Figure 9 (a) and 9 (b) show an AFM 3-D surface view of latex spheres in $TiO_2$ films and the section analysis of such films, that resemble a chain of "mountains" one after the other.

**3.2 Removal of PS spheres:** After achieving a monolayer of packed PS spheres in $TiO_2$ films, the template should ideally be easily removed without causing any damage to the $TiO_2$ film matrix. The removal of the PS spheres can be evaluated via AFM and by electrochemical methods (discussed in section 3.3). In AFM, removal is indicated by the appearance of hemispherical nano-wells in the image that mimic the size and shape of the bottom half of the latex sphere. However, this approach may not provide the complete picture because the AFM tip may not be sharp enough to reach the bottom of the nano-wells. Electrochemical methods, which are described later, provide a more accurate way to determine if the PS latex sphere is completely removed. If any residual material remains in the nano-well, the electrochemical properties will reflect this.

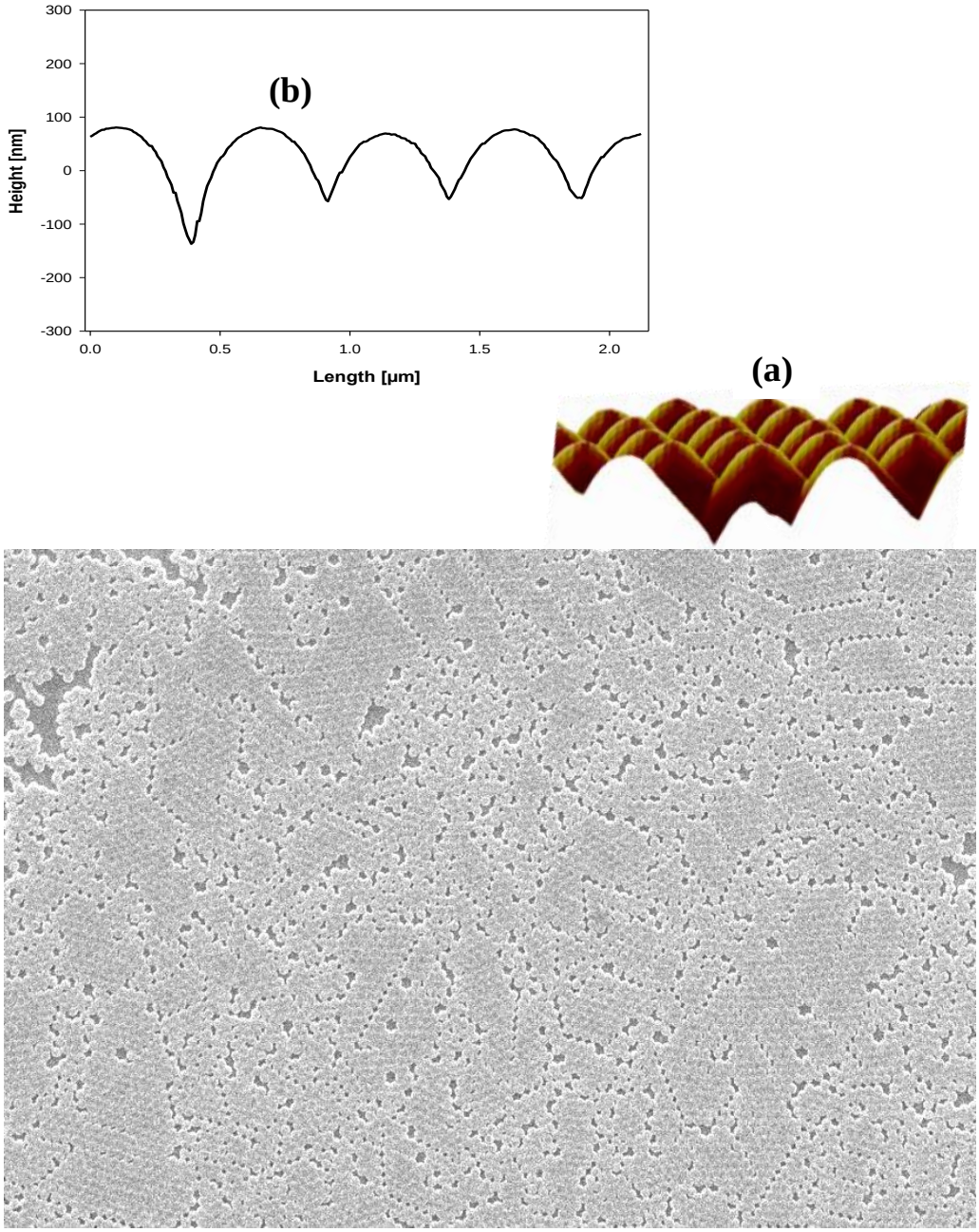


**Figure 9:** A 30 µm x 30 µm SEM image of well-packed monolayer of 470 nm spheres in titania sol spun on an ITO substrate. Inset (a) 1 µm x 1 µm AFM 3D view of PS spheres in the titania matrix. (b) Section analysis of PS spheres in the titania matrix.

The methods tried for removing PS spheres included chemical treatment (toluene, chloroform) and heat treatment (calcination). Chemical treatment is less harsh than heat treatment, and is advantageous to use. Chemical treatment, for example soaking in chloroform for a set period (2 h, 4 h, overnight and one day), resulted in an incomplete removal of the template from the inorganic polymeric matrix, as shown in Figure 10 and as judged by the electrochemical methods (see section 3.3). Heat treatment such as calcination, from room temperature to 435$^{o}$C at 3$^{o}$C ramp and held at 435$^{o}$C for 25 min resulted in successful removal of PS spheres from the inorganic matrix. During calcination, the $TiO_2$ will shrink due to the capillary stress at high temperature and also there is continual condensation and structural relaxation resulting in formation of a more dense matrix around the template which decreases pore dimensions. Calcination at higher temperatures (> 470$^{o}$C) and/or ramping the temperature at a faster rate (> 5$^{o}$C) caused some of the nano-wells to distort as shown in Figure 11. After calcining the PS spheres in a furnace, it is very important to wash the films with distilled water. This removes any residual carbon sticking to the surface and the nanowells in the $TiO_2$ matrix as a result of incomplete combustion during calcination.

The cartoon in Figure 12 shows how the thickness of the films, diameter and depth of the nano-wells are acquired from the AFM images. While the diameter and depths were measured from areas with ordered arrangement of nano-wells, the thickness of the film were measured in an area where there are no nano-wells. Figure 13 shows a 2-D image of nanowells left in the titania matrix after calcination from room temperature to 435$^{o}$C at 3$^{o}$C ramp and held at 435$^{o}$C for 25 min. The inset shows a 3-D surface view of the holes

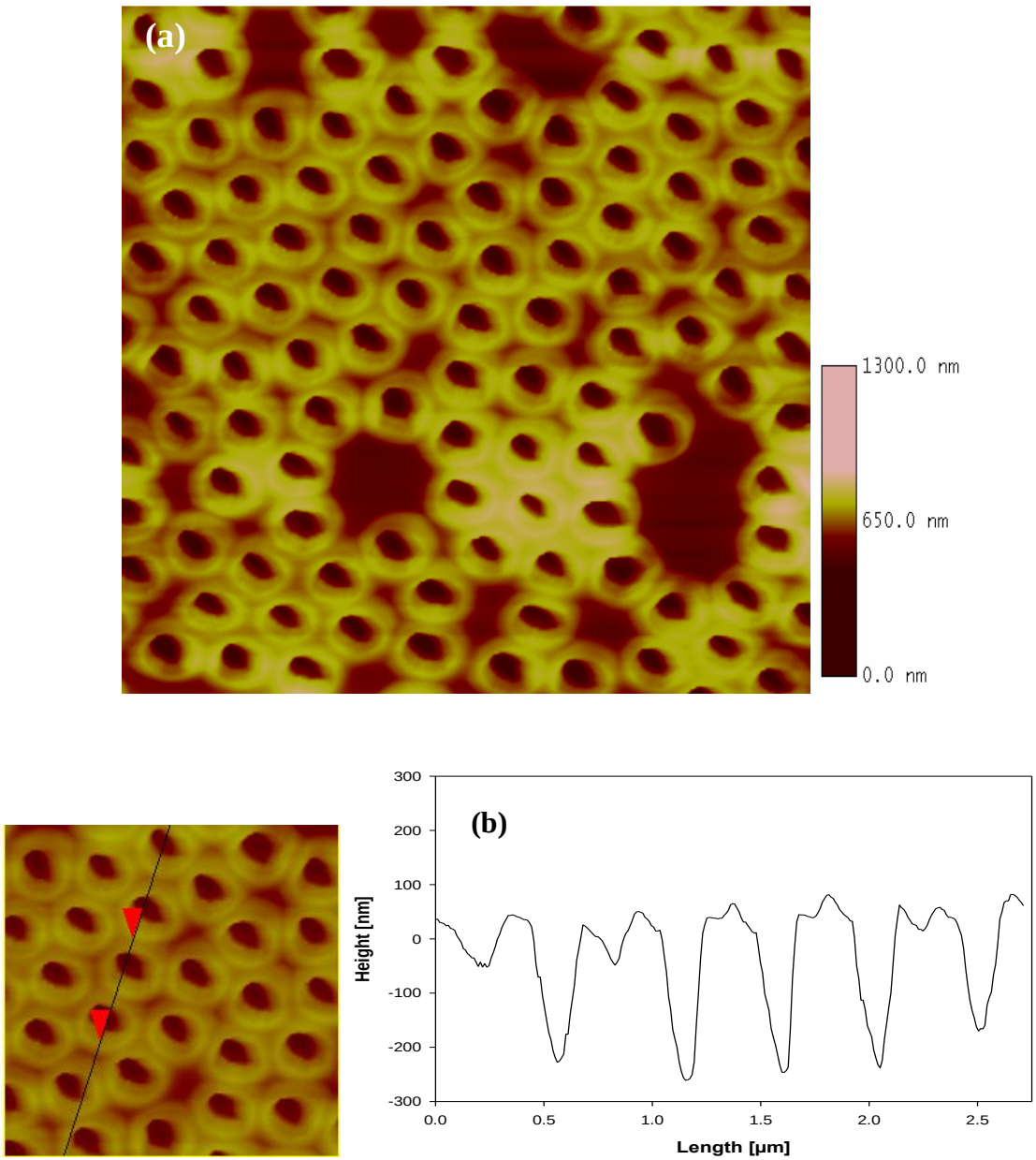


**Figure 10:** (a) A 5 µm x 5 µm AFM image of titania film showing nano-wells after soaking in chloroform for 4 h. (b) Section analysis of the nano-wells in the titania film.

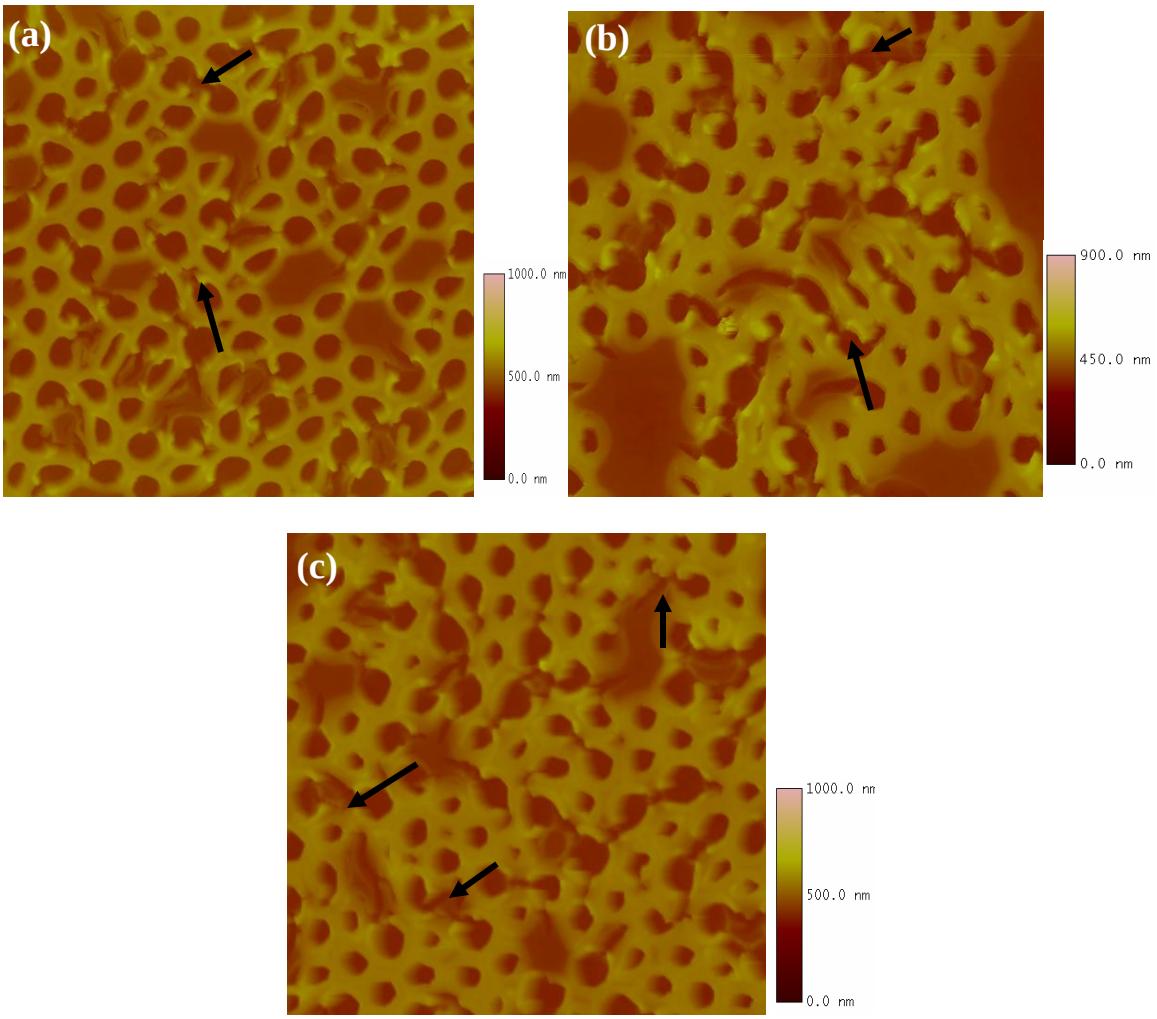


**Figure 11:** A 5 µm x 5 µm AFM images of titania film after calcination from room temperature to (a) 470$^{o}$C at 10$^{o}$C ramp and held at 470$^{o}$C for 40 min (b) 435$^{o}$C at 25$^{o}$C ramp and held at 435$^{o}$C for 40 min (c) 470$^{o}$C at 3$^{o}$C ramp and held at 470$^{o}$C for 40 min. At a faster ramp and higher temperature, distortions of the nano-wells were observed in the film as noted by arrows.

which resemble "wells". The average film thickness, depth and diameter (N = 40) of the nano-wells in the $TiO_2$ matrix after the calcination process were measured to be 28 ± 5 nm, 210 ± 3 nm and 320 ± 10 nm respectively (shown in Figure 14). The average film thickness, depth and diameter (N = 15) of the nano-wells in the $TiO_2$ matrix after soaking in chloroform for 4 h were measured to be 68 ± 4 nm, 321 ± 6 nm and 440 ± 9 nm respectively (shown in Figure 15). When compared to the chemical treatment, for example dissolving in chloroform for 4 h, removing the spheres by calcination resulted in a decrease in diameter, depths and also a change in morphology (as shown in Table 2 and Figure 14 and 15) which is mainly attributed to the shrinking of the matrix due to capillary stress[5] at such high temperatures.

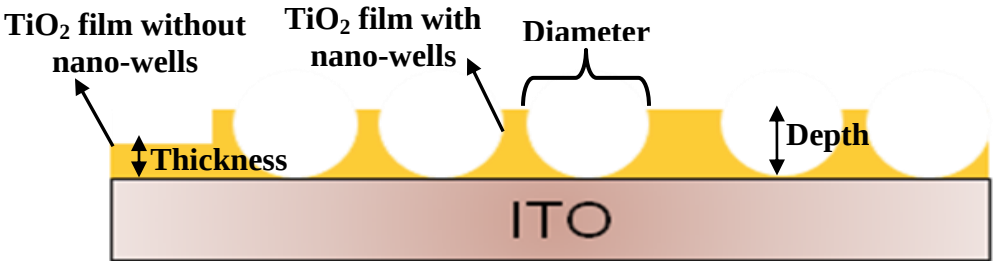


**Figure 12:** Cartoon showing how the thickness of the films, the diameter and the depth of the nano-wells in the film were measured.

**Table 2:** Variations in the thickness of the film, the depth and the diameter of $TiO_2$ nano-wells depending on the methodology used for removing PS spheres.

| Method for removing PS spheres | Depth of nano-wells (nm) | Diameter of nano-wells (nm) | Thickness of the films (nm) |
|---|---|---|---|
| Soak in chloroform for 4 h (N = 15) | 321 ± 6 | 390 ± 9 | 68 ± 4 |
| Calcination (N = 40) | 210 ± 3 | 320 ± 10 | 28 ± 5 |

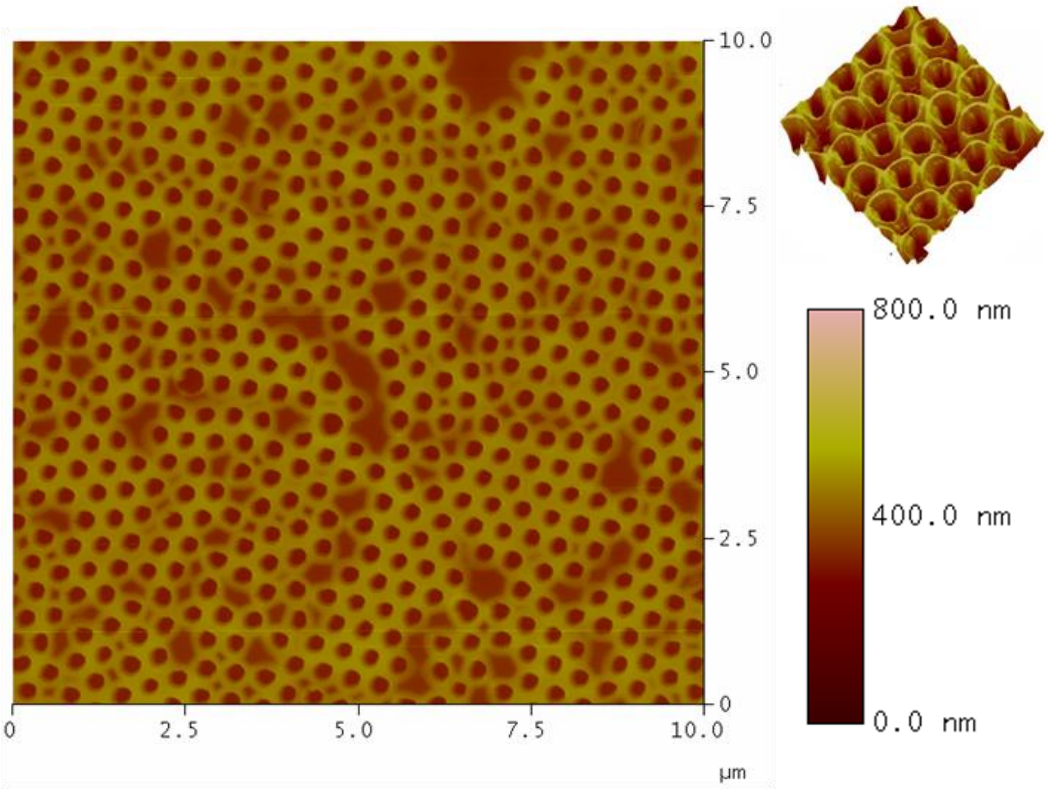


**Figure 13:** A 10 µm x 10 µm AFM image of nano-wells in the titania matrix after calcination from room temperature to 435°C at 3°C ramp and held at 435°C for 25 min. The inset shows a 1 µm x 1 µm AFM 3-D view of the nano-wells.

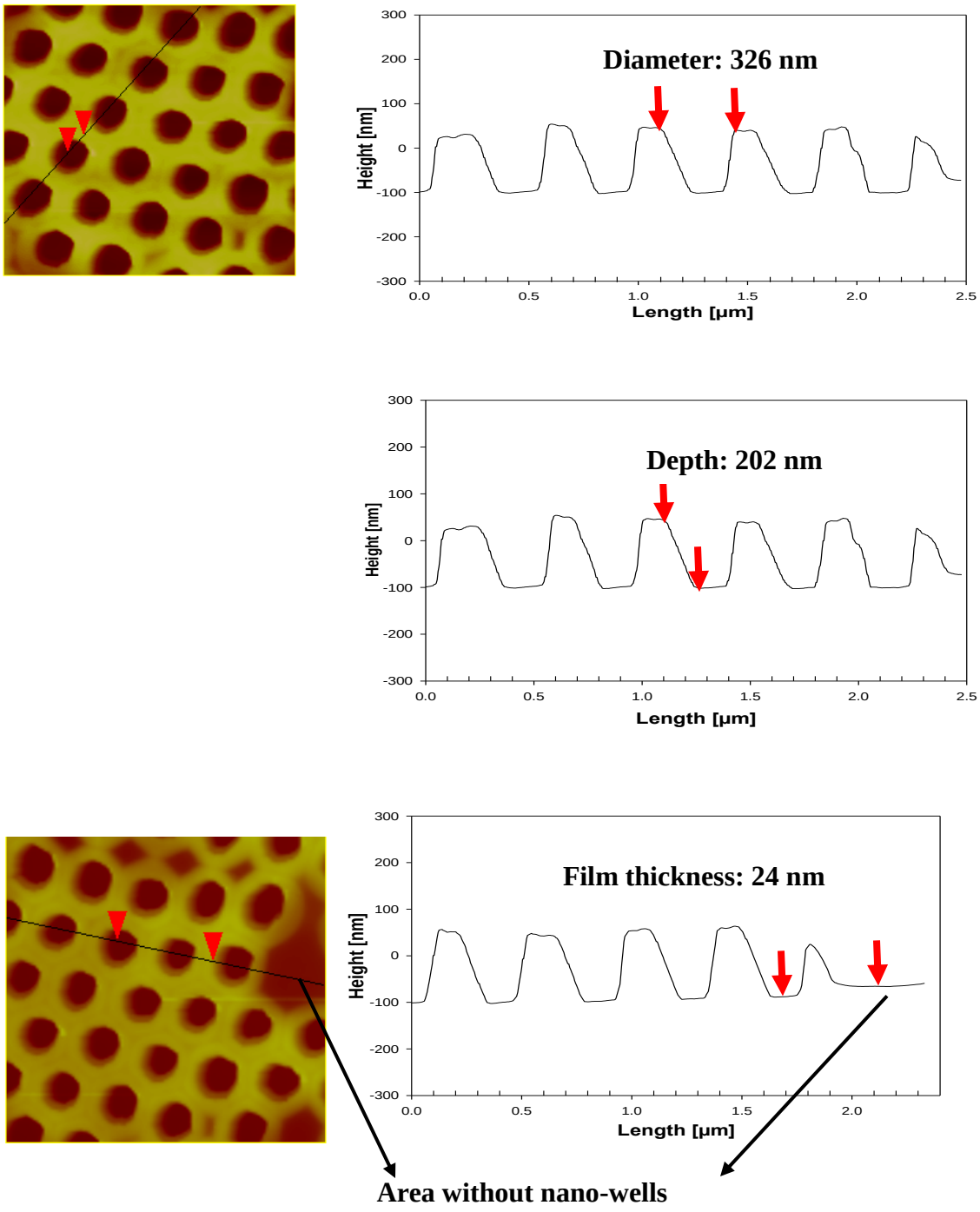


**Figure 14:** Determining the thickness of the $TiO_2$ films, the depth and the diameter of the nano-wells in the titania matrix from a 2.5 µm x 2.5 µm AFM image. The sample was calcined from room temperature to 435°C at 3°C ramp and held at 435°C for 25 min.

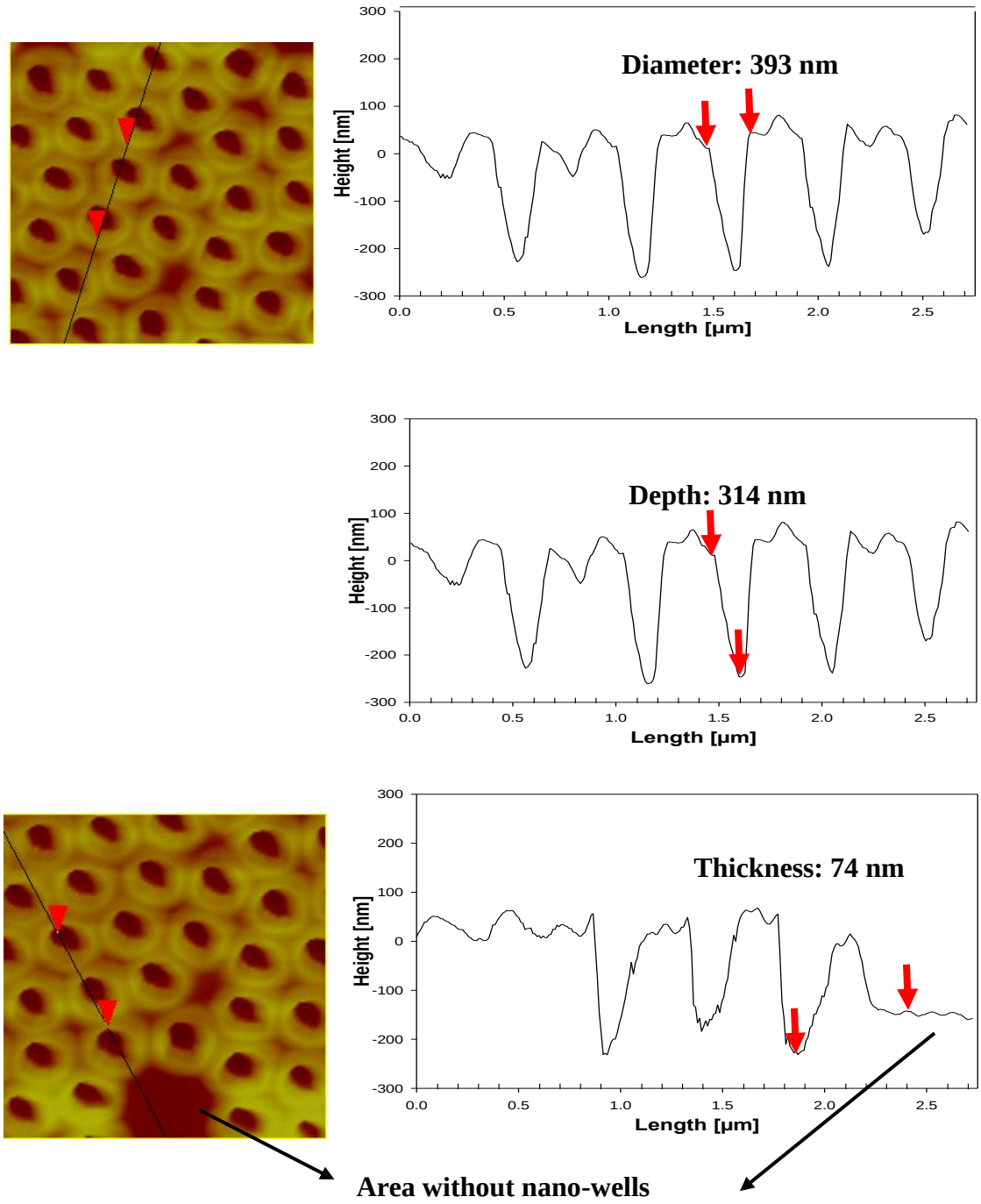


**Figure 15:** Determining the thickness of the $TiO_2$ films, the depth and the diameter of the nano-wells in the titania matrix from a 2.5 µm x 2.5 µm area of a sample after soaking in chloroform for 4 h.

**3.3 Removing defects in the titania films with nano-wells:** When the latex sphere was removed from the film, the underlying electrode (ITO in this case) was exposed. For future experiments, it is important that there is no residual material at the bottom of the nano-wells. Electrochemical techniques can be used to determine if the underlying electrode is exposed.[76] If the nano-wells contain residual material, this can be noted by a change in current relative to control by oxidizing and reducing a redox couple in solution at a particular voltage. However, before these experiments can be done (as well as the future stability studies) it is important to block any defects in the films. Defects develop in the inorganic matrix due to improper packing of the spheres and other factors like imperfections, scratches etc., through which the redox species can reach the underlying substrate as shown in Figure 16 (a). As illustrated in the cartoon shown in Figure 16 (b) it is desirable to block the defects so that electrochemistry only takes place in the nano-wells. One such electrochemical technique wherein the compact nature of the films and the diffusion of redox molecules through the templated films can be studied is cyclic voltammetry (CV).[101]

**3.3.1 Cyclic voltammetry:** CV is a versatile technique to study redox reactions occuring at an electrode surface. This method utilizes a three electrode system wherein the potential is varied between the reference and the working electrode and the current between the counter and the working electrode is measured. In these experiments, the potential at the working electrode is swept back and forth between two values which, when plotted against the current measured, gives the cyclic voltammogram. Figure 17 shows the voltammogram

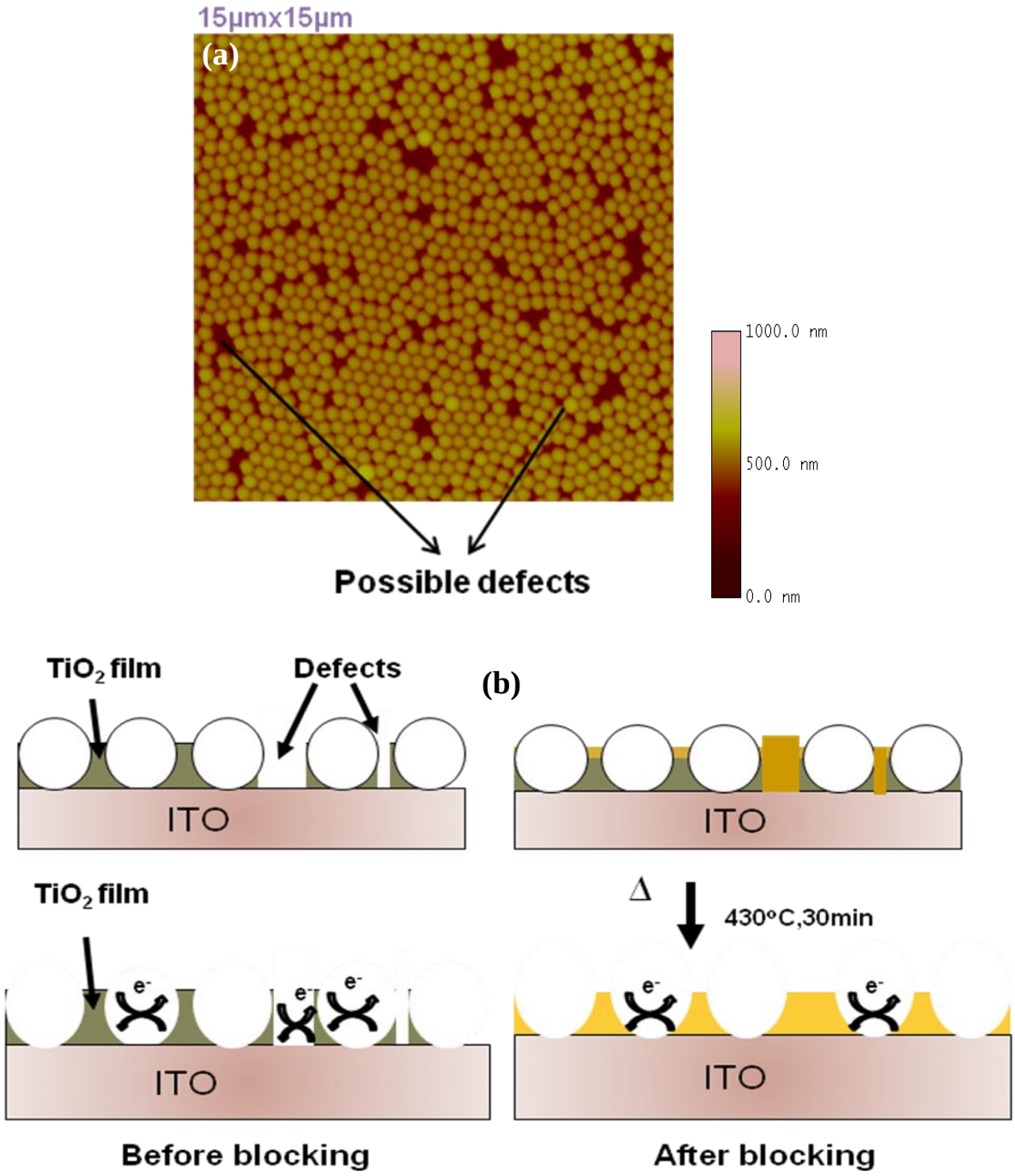


**Figure 16:** (a) A 15 µm x 15 µm AFM image of titania films doped with PS spheres showing possible defects. (b) A cartoon showing effects before and after blocking defects on the electrochemical reactions at the film surface. Not drawn to scale.

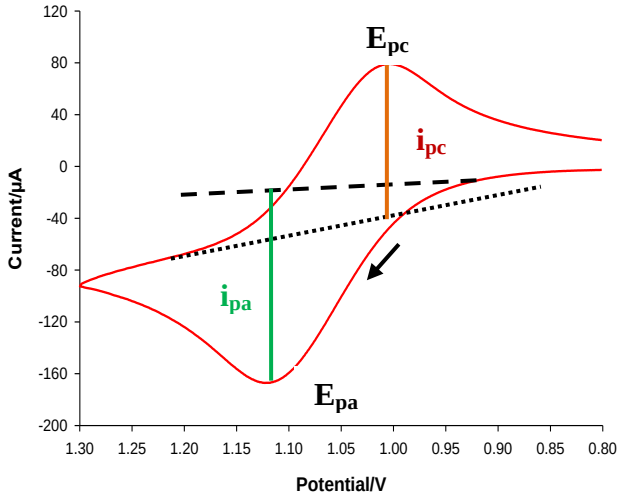


**Figure 17:** A typical cyclic voltammogram of 1mM $[Ru(bypy)_3]^{2+}$ in 0.1 M KCl using a conventional three electrode system with a scan rate 0.1 V/s.

for the reduction of $[Ru(bypy)_3]^{2+}$ in an unstirred solution of 0.1 M KCl using a conventional three-electrode system. The working electrode was an ITO electrode and the reference electrode was Ag/AgCl (1M KCl). A platinum wire was used as a counter electrode. The peak that appears ~ 1.1 V in the forward scan is called the anodic peak and it corresponds to the oxidation of $[Ru(bypy)_3]^{2+}$ to $[Ru(bypy)_3]^{3+}$. The peak at ~ 1.0 V in the reverse scan is called the cathodic peak and it corresponds to the reduction of $[Ru(bypy)_3]^{3+}$ to $[Ru(bypy)_3]^{2+}$. During the forward scan, anodic current develops due to the oxidation of $[Ru(bypy)_3]^{2+}$ at the electrode surface due to the electrode reaction shown below, and continues to increase as the flux of $[Ru(bypy)_3]^{3+}$ increases at the electrode surface.

$$[Ru(bypy)_3]^{2+} \rightarrow [Ru(bypy)_3]^{3+} + e^-$$

When the surface concentration of $[Ru(bypy)_3]^{2+}$ at the electrode surface approaches zero, the anodic current reaches a maximum. The current then decays as the diffusion layer around the electrode surface becomes depleted of $[Ru(bypy)_3]^{2+}$. When the scan is

reversed at a particular voltage, the cathodic current is generated due to the reduction of $[Ru(bypy)_3]^{3+}$ by the following process at the electrode surface:

$$[Ru(bypy)_3]^{3+} + e^- \rightarrow [Ru(bypy)_3]^{2+}$$

The cathodic current continues to increase as the flux of $[Ru(bypy)_3]^{3+}$ increases to the electrode surface. When the surface concentration of $[Ru(bypy)_3]^{3+}$ at the electrode surface approaches zero, the cathodic current reaches a maximum. The cathodic current then decays as the diffusion layer around the electrode surface becomes depleted of $[Ru(bypy)_3]^{3+}$. The current at the end of the reverse scan is not the same as the initial current in the forward scan because not all $[Ru(bypy)_3]^{3+}$ is reduced back to $[Ru(bypy)_3]^{2+}$ because of diffusion. For an electrochemical reversible redox couple, such as $[Ru(bypy)_3]^{3+/2+}$, the peak current is directly related to the concentration of the analyte by Randles-Sevcik equation as shown in the following Equation:[133]

$$i_p = 2.69 \times 10^5 \, n^{3/2} \, A \, D^{1/2} \, C \, v^{1/2}$$

where $i_p$ is peak current, n is number of electrons, A is electrode area in ($cm^2$), D is diffusion coefficient of the redox probe in ($cm^2/s$), C is initial concentration of the redox probe in $mol/cm^3$ and *v* is scan rate in V/s. The ratio of the anodic to cathodic peak current ($i_{pa}/i_{pc}$) for a simple reversible redox couple is unity. The peak currents are measured by extrapolating to the preceding baseline current. The anodic ($E_{pa}$) and cathodic ($E_{pc}$) peak

potentials are related to the formal potential ($E^o$) of the redox process. The formal potential for a reversible couple is the center of $E_{pa}$ and $E_{pc}$:[133]

$$E° = (E_{pa} + E_{pc})/ 2$$

The difference between the anodic and cathodic peak potentials for a reversible redox couple is given by the equation below. Thus, the peak separation ($\Delta E_p$) can be used to determine the number of electrons transferred as long as the reaction is reversible.

$$\Delta E_p = E_{pa} - E_{pc} = 59 \text{ mV}/n$$

The characteristics of CV depend on a number of factors like the size of the electrode, voltage scan rate, rate of the electron transfer reaction and rate of mass transfer of the redox species to the electrode surface. For a totally reversible one-step, one-electron reaction process at the planar electrode surface, mass transport is generally assumed to be that of linear diffusion. The shape of the CV for such an electrode, show a peak shaped graph as shown in Figure 18 (a). At electrodes with smaller dimensions such as ultramicroelectrodes (UME), the electrode area is much smaller than the diffusion layer developed during mass transport. The mass transport to the ultramicroelectrode surface occurs via radial diffusion. At longer times, where the diffusion-layer thickness is large compared to the electrode dimension, steady state current is achieved and given by the following equation:

$$i_{ss} = 4nFDCr$$

where $i_{ss}$ is steady state current, n is number of electrons, D is diffusion coefficient of the redox probe in ($cm^2/s$), C is the initial concentration of the redox probe in $mol/cm^3$ and r is the radius of the UME.[133, 134] The CV at an UME is sigmoidal shaped curve as shown in Figure 18 (b).

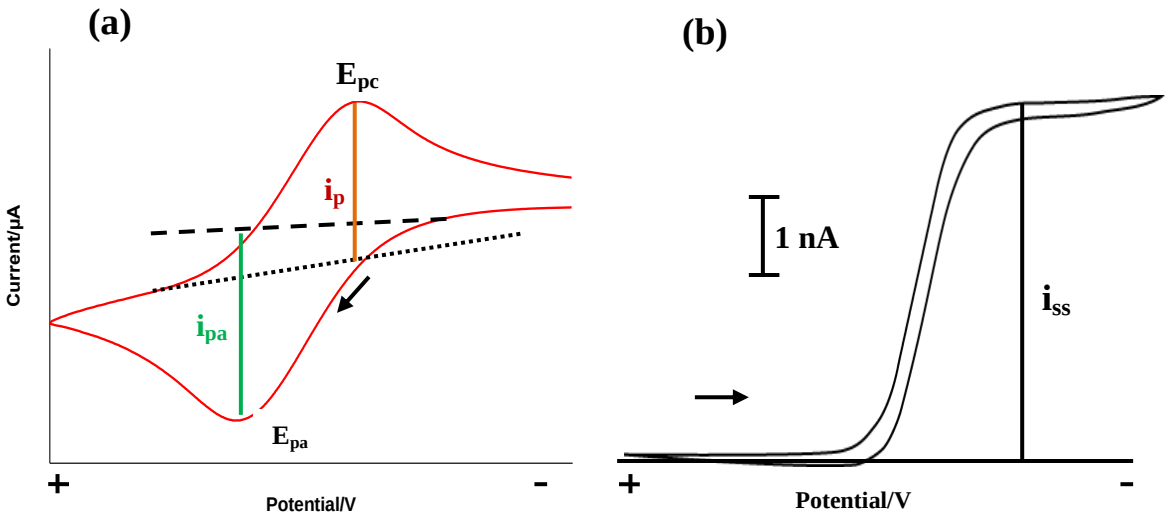


**Figure 18:** A representative CV of a reversible electroactive species at a (a) planar electrode and an (b) ultramicroelectrode (UME) at slow sweep rates.[133]

**3.3.2 Chemically modified electrodes:** To explain the voltammetry at the titania and silica films on ITO, it is important to understand the fundamentals of electrochemical processes at chemically modified electrodes.[135] Electrodes that are either modified with an electroactive monolayer or a film are termed chemically modified electrodes. In our studies, we deal with thin titania films on a conducting ITO substrate. The presence of the $TiO_2$ films on the ITO surface will influence the electrochemical behavior (shape and current) of a redox molecule in solution at an electrode surface. For example, if the

electrode is modified with a film with little to no porosity, the redox species will not be able to diffuse through the film and exchange electrons with the underlying substrate. As a result, no Faradic current would be measured as shown in Figure 19 (a). In another case, when a non-porous film on the electrode surface has many defects that are closely spaced together, the diffusion of the electroactive species would be similar to that of a planar electrode (linear diffusion) as shown in Figure 19 (b). The reason for the increase in Faradaic current is that the diffusion layer of the species at the numerous closely spaced defects overlaps resulting in electrochemical behavior that is similar to that observed at a large uncoated electrode. When the defects are far apart, each of the defects act like an ultra-microelectrode and the mass transport of the redox species to the electrode would be in a radial manner. The CV's of such electrodes are sigmoidal in shape as the potential is swept back and forth between two values as shown in Figure 19 (c).

**3.3.3 Cyclic voltammetry before and after blocking the defects:** To fully evaluate the electrochemistry on an electrode modified with templated $TiO_2$ films, the defects formed during spin-coating should be blocked. Initially, before template removal, the CV of ferrocene methanol at the titania film with PS spheres is peak shaped due to the numerous defects present in the matrix as shown in Figure 20. If no defects are present, no Faradaic current would be observed. To study the voltammetry only in the nano-wells, these defects need to be blocked. So, ideally after the defects are blocked, the CV of the film with well-packed PS spheres should not give any Faradaic current.

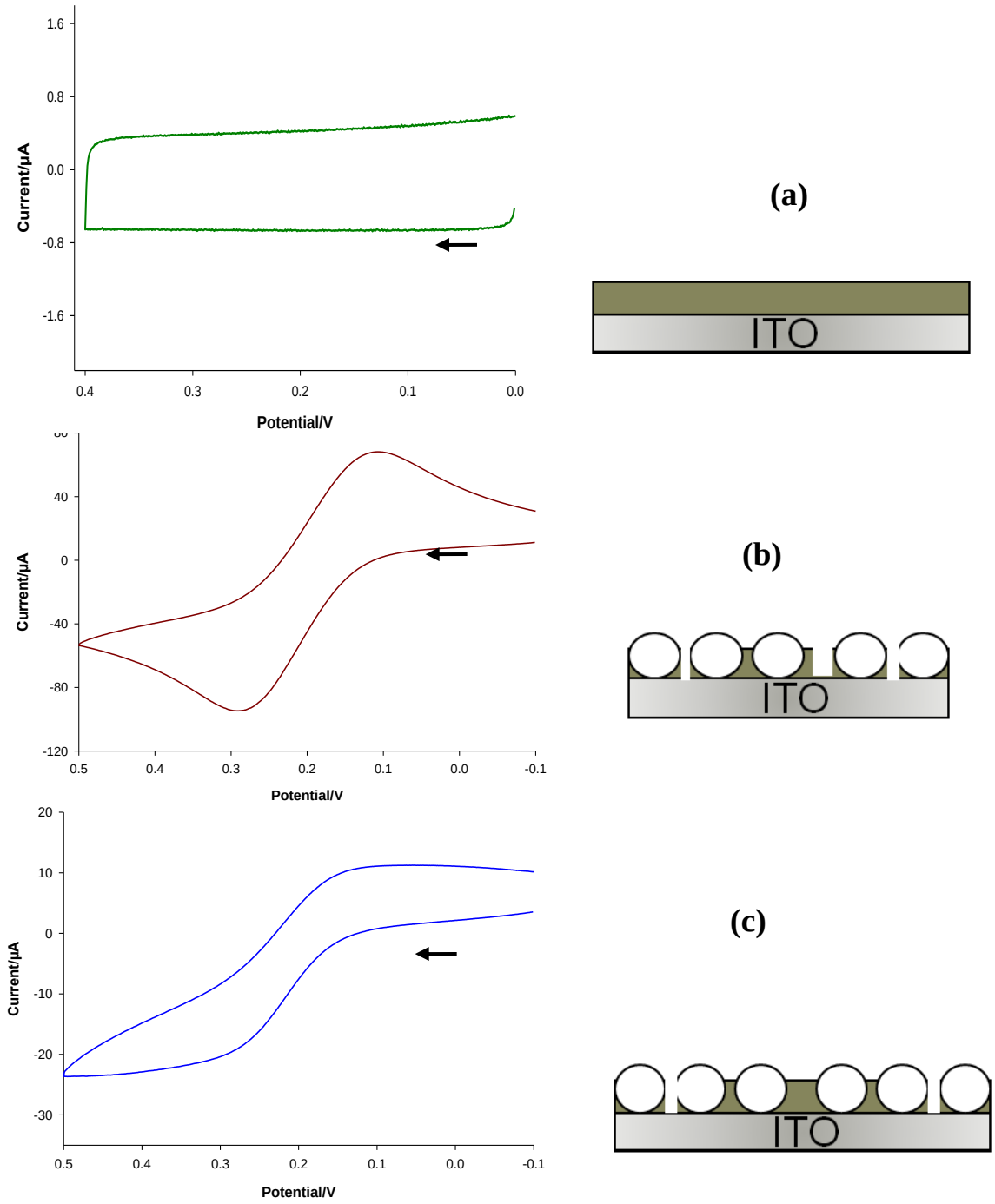


**Figure 19:** CV's of 1 mM $FcCH_2OH$ at electrodes modified chemically with (a) a complete insulating non-porous film (b) non-porous film with numerous closely spaced defects (c) non-porous film with few defects that are far apart.

To confine the electrochemistry to the nano-wells, two different methods were tested to block the defects. The first method was proposed by the Collinson group wherein the defects were blocked by soaking a silicate film doped with spheres in a solution of octyl-trimethoxysilane for two hours.[76] A similar procedure applied to PS spheres in titania films was unsuccessful. Figure 21 shows the CV's of $FcCH_2OH$ at an electrode modified with a layer of PS spheres in titania film before and after blocking with octyl-TMOS. A considerable Faradaic current was noticed on the blocked films with PS spheres, and the current was comparable to films before blocking, indicative of the film not being blocked consistently.

As mentioned earlier, it is important to note that the absolute values of current from the CV's cannot be compared because the areas of the electrode in the redox probe solution are different. However, the changes in shape and the shift in $\Delta E_p$ of different samples (or electrodes) can be compared. Another method tried for blocking the defects involved casting a dilute sol of $TiO_2$ complexed with ACAC and this was successful. Figure 22 shows the CV's of 1 mM $FcCH_2OH$ at a bare ITO slide and an electrode modified with a film containing closely packed spheres before and after blocking the defects. The CV before blocking shows significant Faradaic curent and a traditional diffusion controlled peak shape that is similar to a bare electrode. In contrast, the CV after blocking showed no significant Faradaic current. The increase in Faradaic current at electrodes coated with films containing PS spheres before blocking is attributed to the presence of closely existing defects in titania films. The diffusion layer of the $FcCH_2OH$ at each defect overlaps resulting in a CV that resembles one obtained at a single large bare electrode. Whereas the

CV of the film blocked after spinning a dilute sol of $TiO_2$ have no defects in the titania film so the redox species cannot diffuse through the film to the electrode surface.

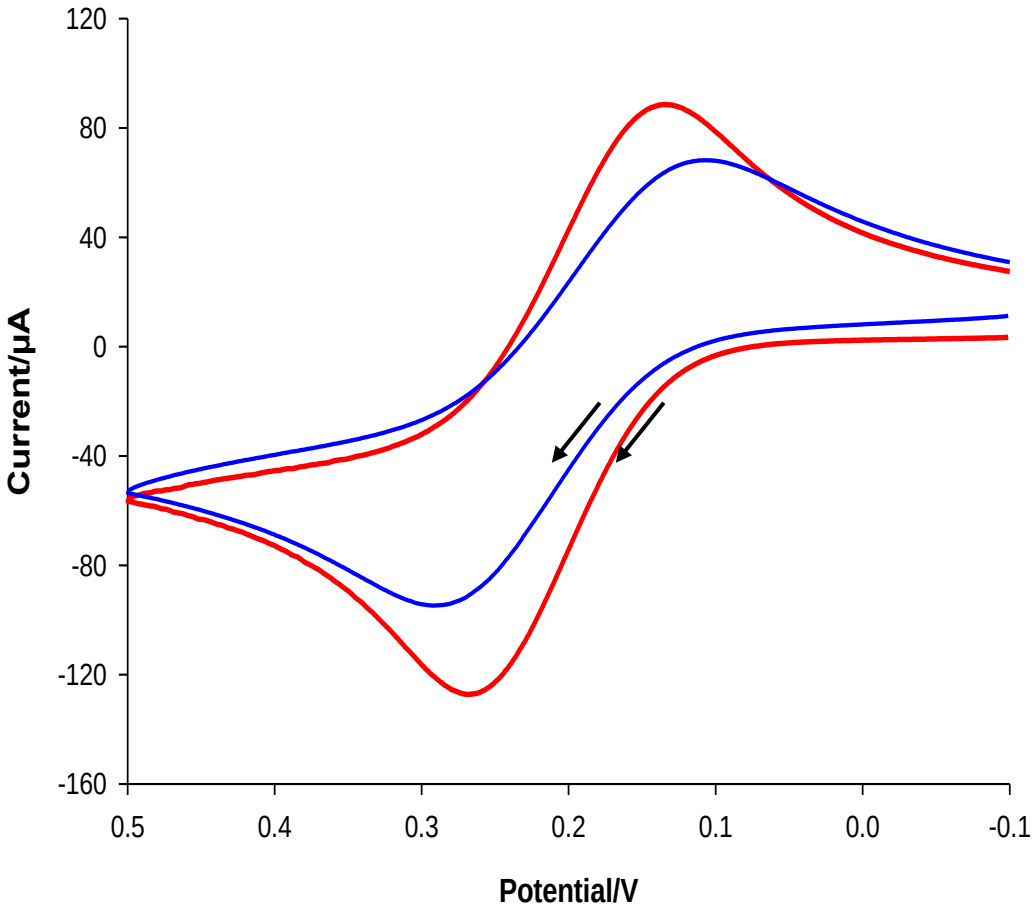


**Figure 20:** CV's of 1 mM $FcCH_2OH$ in 0.1 M KCl at the bare electrode (red) and titania films containing PS spheres before blocking (blue). Scan rate 0.1 V/s. Numerous defects are present as evidenced by the similarity in shape and peak current to the bare electrode.

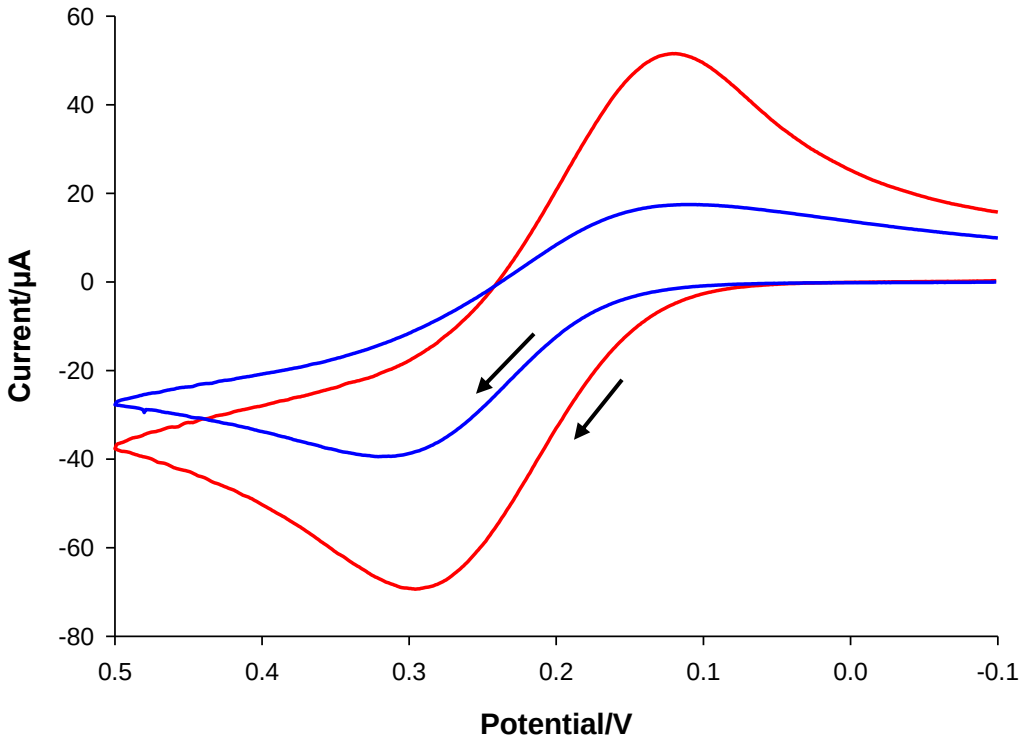


**Figure 21:** CV's of 1 mM $FcCH_2OH$ in 0.1 M KCl at the titania films with PS spheres blocked by soaking in octyl-TMOS (blue) compared to the titania films with PS spheres before blocking (red). Scan rate 0.1 V/s. Some defects are blocked as evidenced by the significantly smaller current and sigmoidal shape of the CV, but many defects remain.

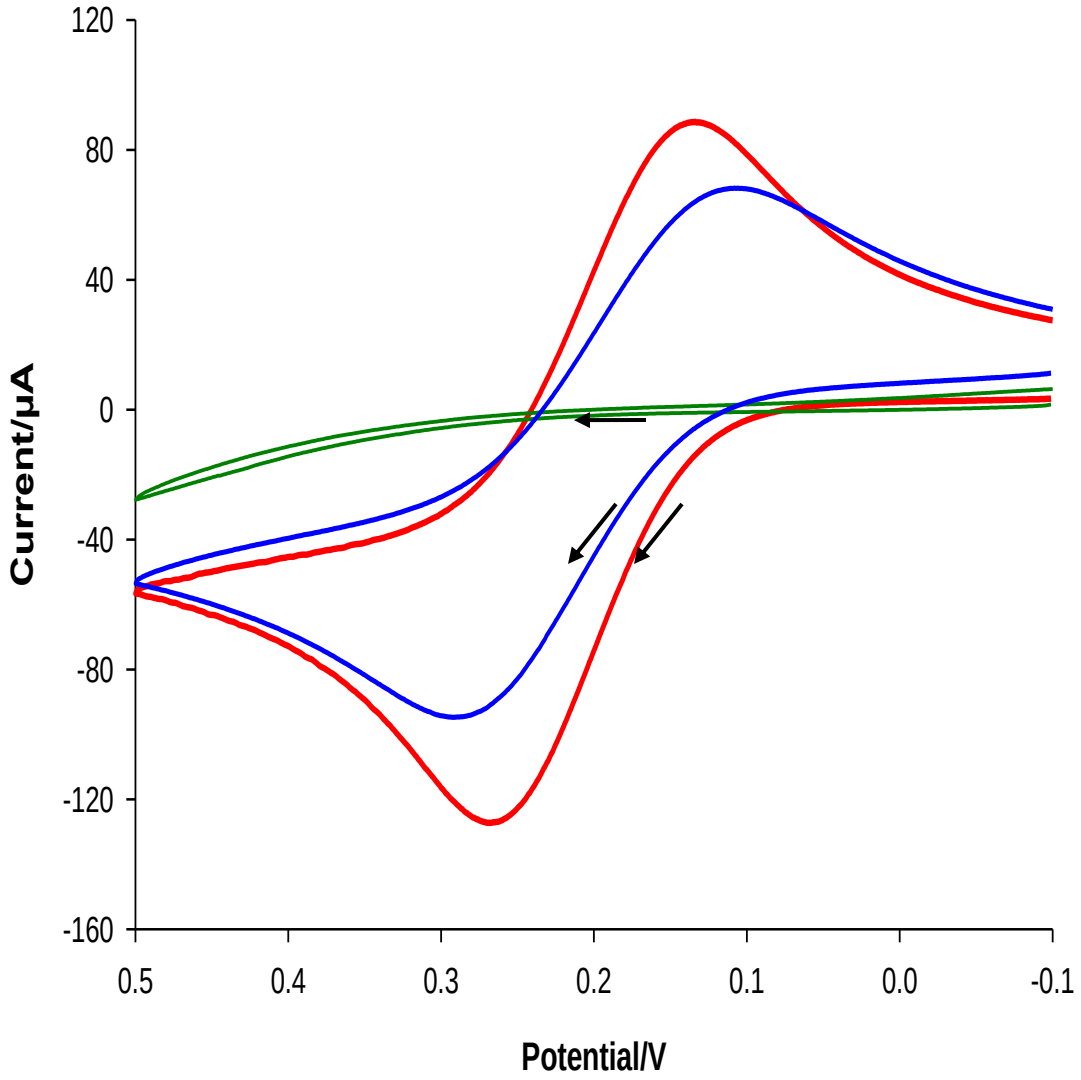


**Figure 22:** CV's of 1 mM $FcCH_2OH$ in 0.1M KCl at the bare electrode (red), titania films with PS spheres before blocking (blue) and films with PS spheres after blocking with a dilute titania sol (green). Scan rate 0.1 V/s. Most defects are blocked as evidenced by the significantly lower Faradaic current compared to the bare electrode or with the film containing spheres before blocking.

**3.4 Stability studies:** Some of the factors which play an important role in preparing stable films are sol sitting time, drying time and the drying conditions i.e., humidity. The effect of these parameters on the stability of the films can be evaluated using an electrochemical technique like cyclic voltammetry. Earlier work of Collinson and co-workers showed that the silica films dried at lower humidity for longer time resulted in more stable films. The CV's of such films when placed in a supporting electrolyte solution containing a redox probe showed no Faradaic current on day one. As the silica film sat in the electrolyte solution for more time, defects developed resulting in a peak shaped CV. [101]

Figure 23 shows a comparison of CV's of sphere doped titanium films after drying at 20 % (approx.) relative humidity (RH) for two hours and two days. The relative humidity was controlled by drying the films in an oven and the value ranges between 15-20 %. A observed in this Figure, the voltammetric response of films dried for two hours shows sigmoidal shaped CV, attributed to the presence of few defects in the films reulting from incomplete drying. Whereas titania films dried for two days at 20 % RH showed no Faradaic current indicative of no defects in the film matrix.

As discussed earlier, after drying the films containing spheres (all defects blocked), the template was removed either by soaking in chloroform or calcination leaving nano-wells in the film surface. Figure 24 shows the CV's of $FcCH_2OH$ at a (1) bare ITO electrode, (2) blocked $TiO_2$ film containing PS spheres and (3) blocked $TiO_2$ film after removing the spheres via soaking in chloroform for four hours. It is evident from the CV that soaking in chloroform for four hours did not completely remove the spheres as there is not much change in the Faradaic current nor shape when compared to the titania films that contain

spheres. This indicates that though the nano-wells are open (as observed via AFM) from the top, there is still residual material at the bottom, blocking electron transfer. Figure 25 shows the CV's of 1 mM $FcCH_2OH$ at a bare ITO electrode, blocked $TiO_2$ film with spheres and blocked $TiO_2$ film after the spheres are removed via calcination. As can be observed in Figure 25, the voltammetry of the film after template removal shows a similar peak shape as that obtained on a bare substrate, indicating a complete removal of the PS spheres. Faradaic current is observed due to the diffusion of redox species through the nano-wells to the substrate surface. The nano-wells being closely spaced causes the electrode to act as a single big electrode resulting in a peak shaped CV.[101]

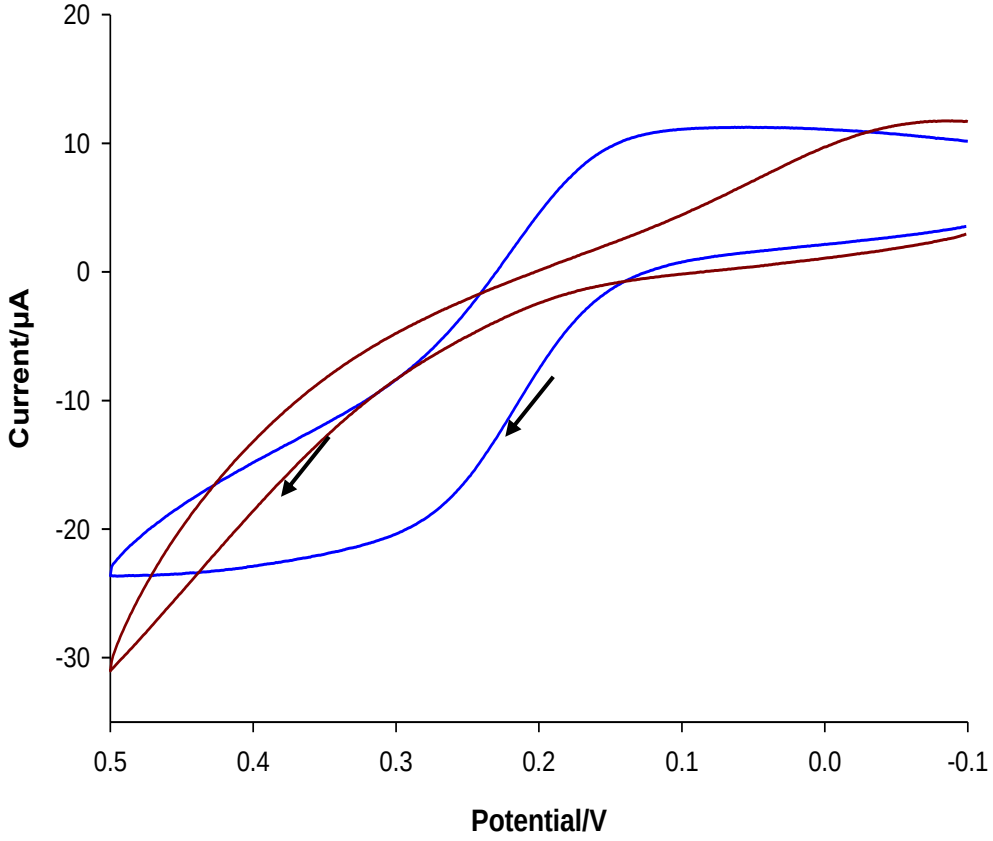


**Figure 23:** CV's of 1 mM $FcCH_2OH$ in 0.1 M KCl at $TiO_2$ films with PS spheres blocked with dilute Ti sol and dried for two hours (blue) and two days in an oven maintained at 36$^{o}$C (brown). Scan rate 0.1 V/s. It can be noticed from the sigmoidal shape of the CV that some defects arise due to incomplete drying of the film when dried for two hours whereas the film dried for longer period (two days) showed significantly lower Faradaic current.

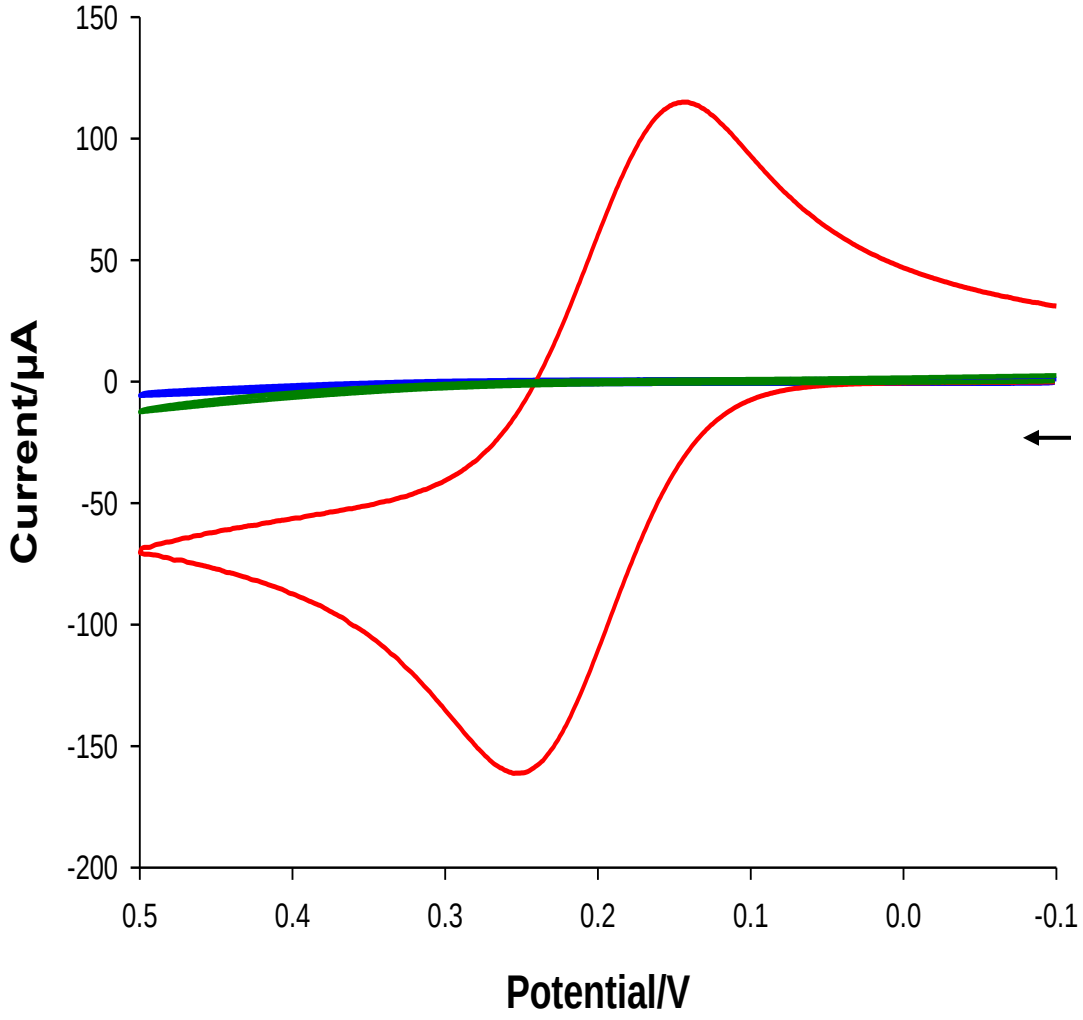


**Figure 24:** CV's of 1 mM $FcCH_2OH$ in 0.1 M KCl at a bare electrode (red), blocked titania films with PS spheres (green) and blocked titania films after removal of PS spheres via soaking in chloroform for 4 h (blue). Scan rate 0.1 V/s. It can be noticed from the CV that the films after soaking in chloroform shows no significant change in the Faradaic current indicating presence of residue at the bottom of nano-well.

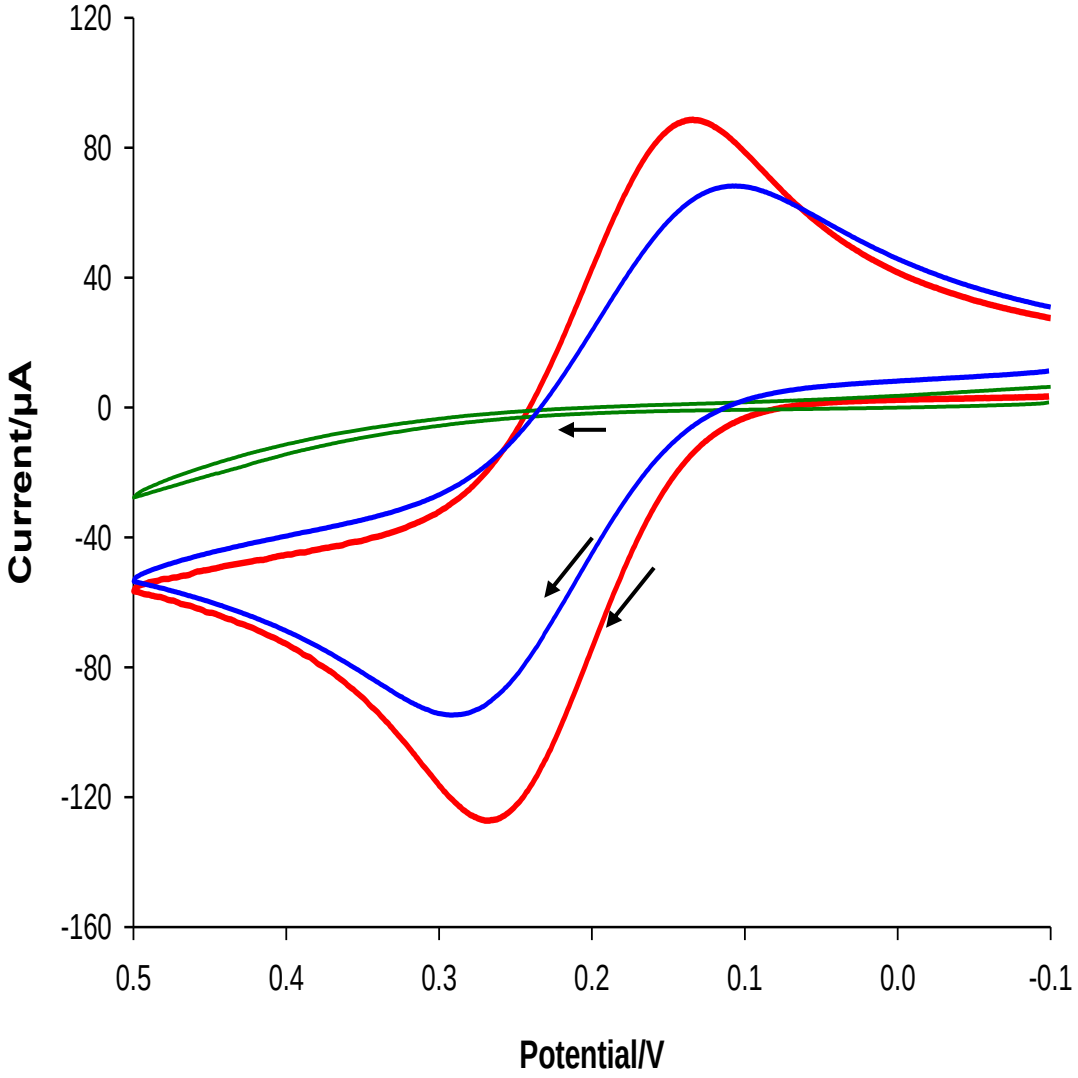


**Figure 25:** CV's of 1 mM $FcCH_2OH$ in 0.1 M KCl at a bare electrode (red), blocked titania films with PS spheres (green) and blocked titania films after removal of PS spheres via calcination (blue). Scan rate 0.1 V/s. The CV of the film after calcination shows a peak shaped graph similar to that observed at the bare electrode indicating that the nano-wells are open.

To evaluate the stability of the $TiO_2$ films, the blank ITO and the films containing spheres and nano-wells were soaked in 0.1 M KCl for a period of two months. Cyclic voltammetry was used to study the changes in Faradaic current of the redox probe in solution at the electrode surface. An ideal probe for the stability studies should have fast electron transfer kinetics and be chemically and electrochemically reversible. The redox molecule can reach the underlying surface either by diffusion or partitioning into the film.[9] To determine whether the transport of the redox species through the films to the underlying substrate will be affected by the type of charged species (cation, anion or neutral), the CV's of the films were obtained using redox molecules having different charges. It was observed by Collinson and co-workers that when the charge of the film and the redox probe are the same, the redox probe cannot easily diffuse across the film resulting in very little Faradaic current. In another case, when the film and the redox probe have opposite charges, the redox probe ion-exchanges to some extent into the film due to which higher current when compared to neutral probe is observed.[9] To study these charge dependent effects in the transport of redox species across the titania films, three redox probes, ferrocene methanol ($FcCH_2OH$), potassium ferricyanide [$Fe(CN)_6^{3-}$] and tris (2,2'-bipyridyl) dichlororuthenium (II) hexahydrate ([$Ru(bypy)_3]^{2+}$) (different type of charged species) were used. However, in the preparation of titania films, the pH of the amine-complexed sol is close to the isoelectric pH (net charge zero) of titania. As a result, films will have a neutral charge and hence it is expected that these charge dependent effects will not be observed. The oxidation reactions of these probes in solution when the potential is applied in a positive direction are given below:

$$FcCH_2OH \rightleftharpoons Fc^{+}CH_2OH + 1e^{-}$$

$$Fe(CN)_6^{4-} \rightleftharpoons [Fe(CN)_6]^{3-} + 1e^{-}$$

$$[Ru(bypy)_3]^{2+} \rightleftharpoons [Ru(bypy)_3]^{3+} + 1e^{-}$$

The films placed in water have a probability of forming hydroxyl groups (from the interaction of $OH^{-}$) by breaking the Ti-O-Ti bonds and forming Ti-OH bonds. These structural rearrangements in the films result in formation of intrinsic defects within the matrix that eventually result in the film falling off the substrate surface. Cyclic voltammetry can be used to study the formation of defects in the films after soaking in 0.1 M KCl, which will be noticed as an increase in Faradaic current. Titania films containing nano-wells cannot be used for stability tests because the Faradaic current from the nano-wells and the defects developed cannot be distinguished. However, titania films with spheres wherein all the defects are blocked can be used to study the stability of the films after soaking in 0.1 M KCl. Any changes in the structure of the titania films with spheres (leading to defects) can be reflected as an increase in current during the voltammetric experiments. The CV's of $FcCH_2OH$, $Fe(CN)_6^{3-}$ and $[Ru(bypy)_3]^{2+}$ (in solution) at the surface of $TiO_2$ films containing spheres showed negligible Faradaic current on day 1, day 15, day 30 and day 60 and they look similar over time (until 60 days) as shown in Figures 26, 27 and 28. This indicates that the films have a stable, compact structure through which no electron transfer takes place. Also, the CV of the samples with nano-wells showed an increase in Faradaic current due to the linear diffusion of the redox probe to the substrate surface.

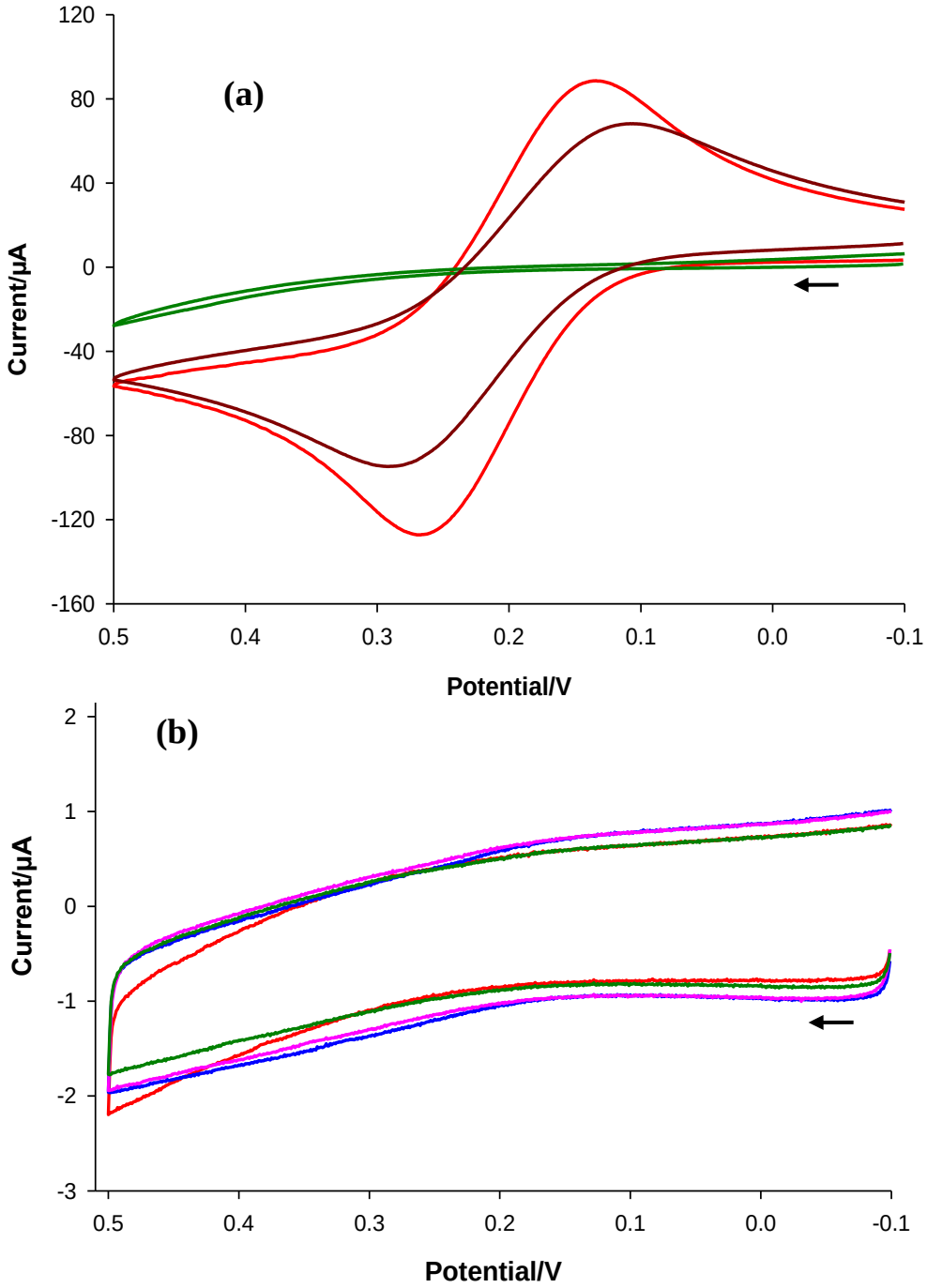


**Figure 26:** (a) CV's of 1 mM $FcCH_2OH$ in 0.1 M KCl at bare electrode (red), "blocked" $TiO_2$ film with PS spheres (green), "blocked" $TiO_2$ film after template (PS) removal (brown) (b) Expansion of the CV's of 1 mM $FcCH_2OH$ in 0.1 M KCl at "blocked" $TiO_2$ films with PS spheres after soaking in 0.1 M KCl for 1 (red), 15 (blue), 30 (pink) and 60 (green) days. Scan rate 0.1 V/s. As observed from the CV's in(b) there is no significant change in Faradaic current over a period of 60 days indicating that no defects arise after soaking in 0.1 M KCl.

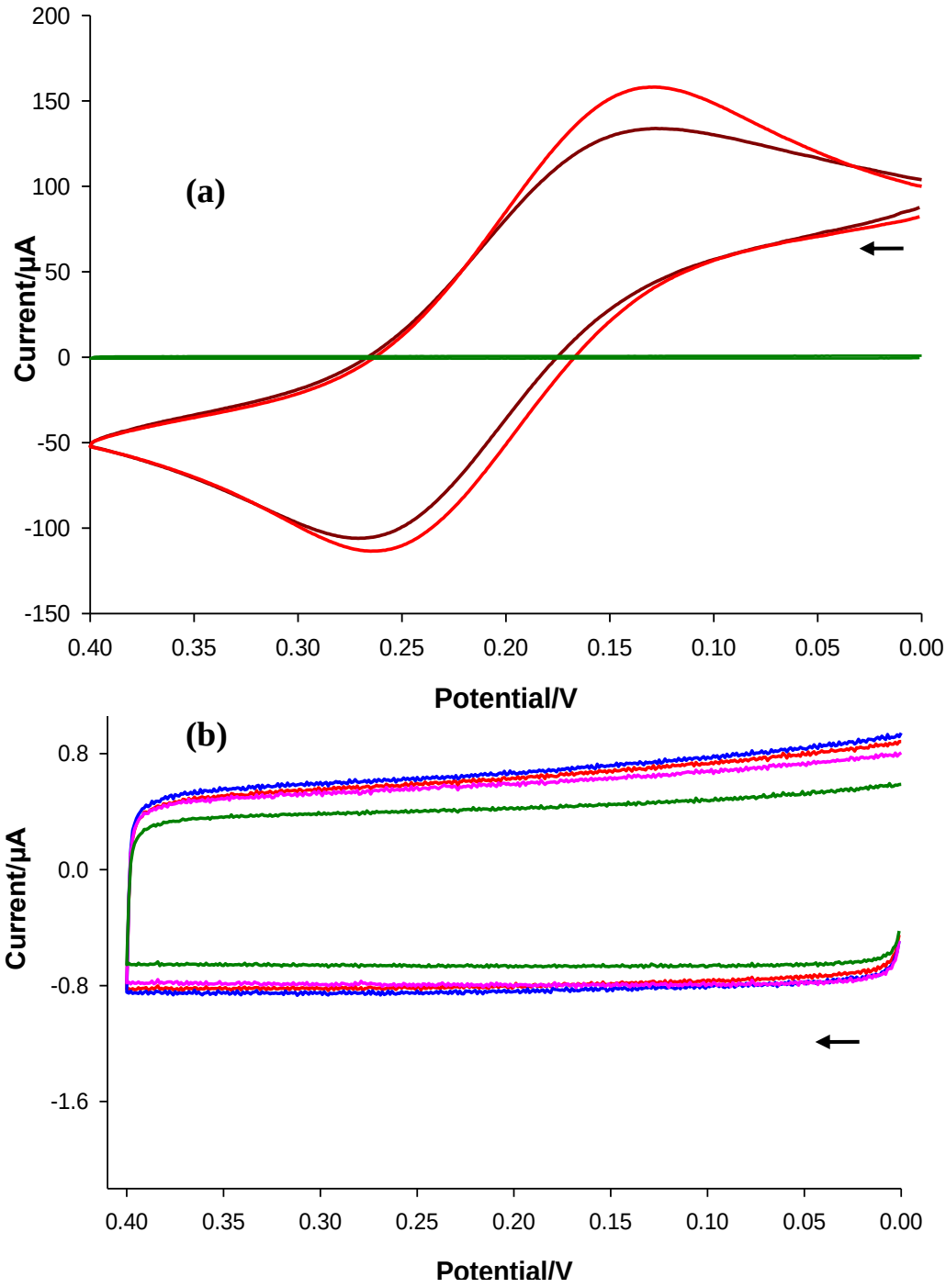


**Figure 27:** (a) CV's of 1 mM $Fe(CN_6)^{3-}$ in 0.1 M KCl at bare electrode (red), "blocked" $TiO_2$ film with PS spheres (green), "blocked" $TiO_2$ film after template (PS) removal (brown) (b) Expansion of the CV's of 1 mM $Fe(CN)_6^{3-}$ in 0.1 M KCl at "blocked" $TiO_2$ films with PS spheres after soaking in 0.1 M KCl for 1 (red), 15 (blue), 30 (pink) and 60 (green) days. Scan rate 0.1 V/s. As observed from the CV's in (b) there is no significant change in Faradaic current over a period of 60 days indicating that no defects arise after soaking in 0.1 M KCl.

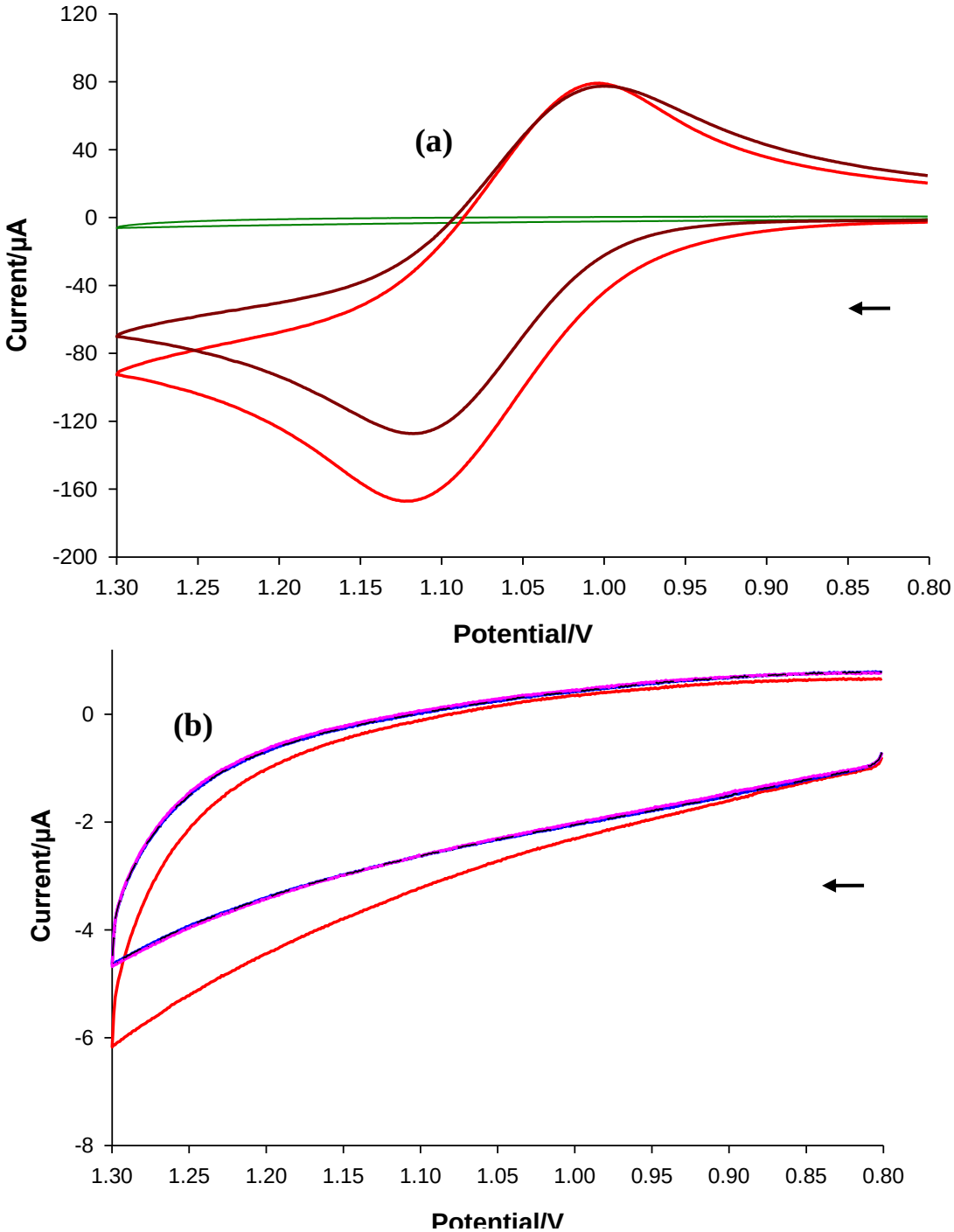


**Figure 28:** (a) CV's of 1 mM $[Ru(bypy)_3]^{2+}$ in 0.1 M KCl at bare electrode (red), "blocked" $TiO_2$ film with PS spheres (green), "blocked" $TiO_2$ film after template (PS) removal (brown) (b) Expansion of the CV's of 1 mM $[Ru(bypy)_3]^{2+}$ in 0.1 M KCl at "blocked" $TiO_2$ films with PS spheres after soaking in 0.1 M KCl for 1 (red), 15 (blue), 30 (pink) and 60 (green) days. Scan rate 0.1 V/s. As observed from the CV's in (b) there is no significant change in Faradaic current over a period of 60 days indicating that no defects arise after soaking in 0.1 M KCl.

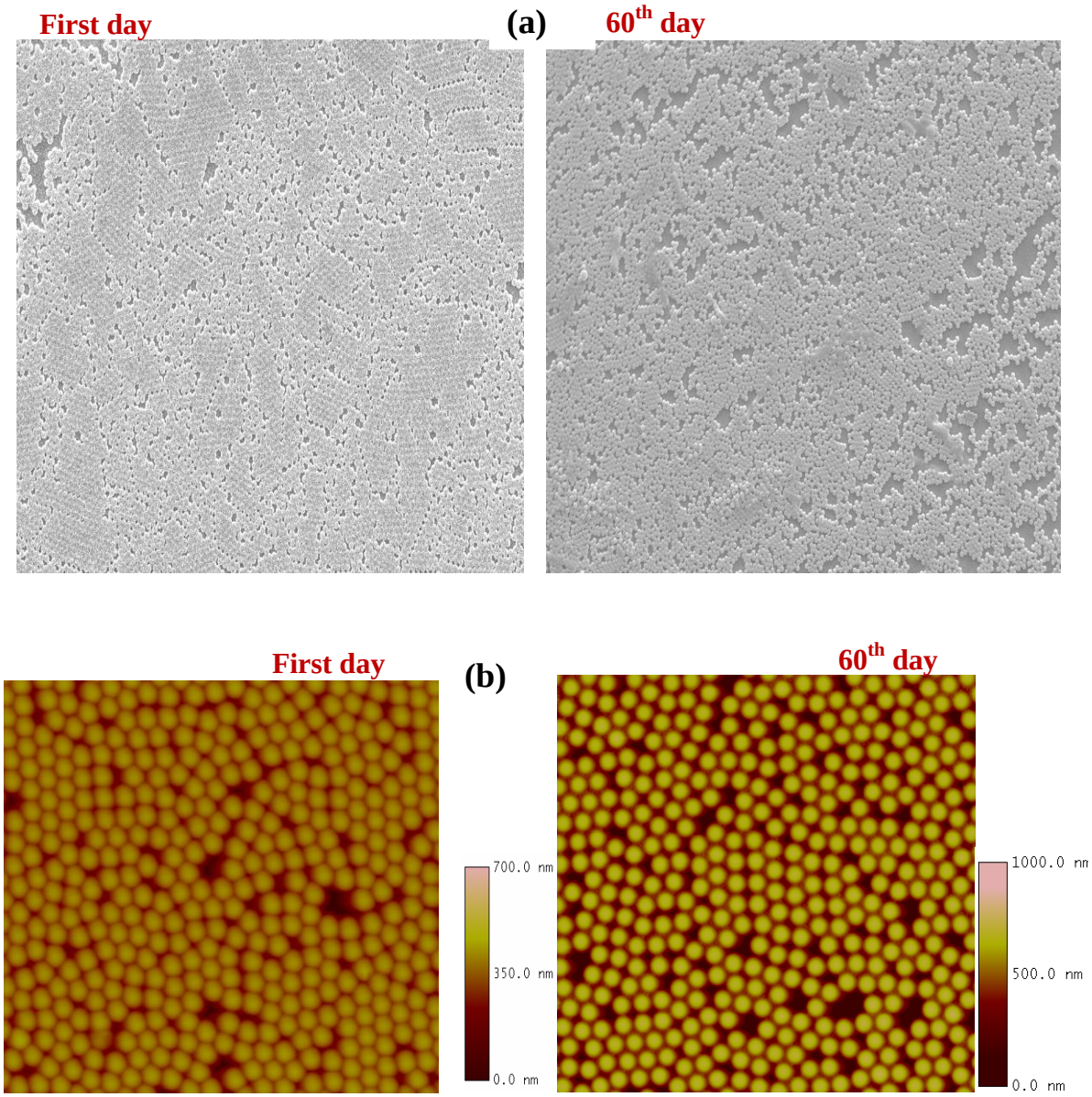


**Figure 29:** (a) 30 µm x 30 µm SEM images of titania film with PS spheres soaked in 0.1 M KCl on first and 60$^{th}$ day (b) 10 µm x 10 µm AFM images of titania film with PS spheres soaked in 0.1 M KCl on first day and 60$^{th}$ day.

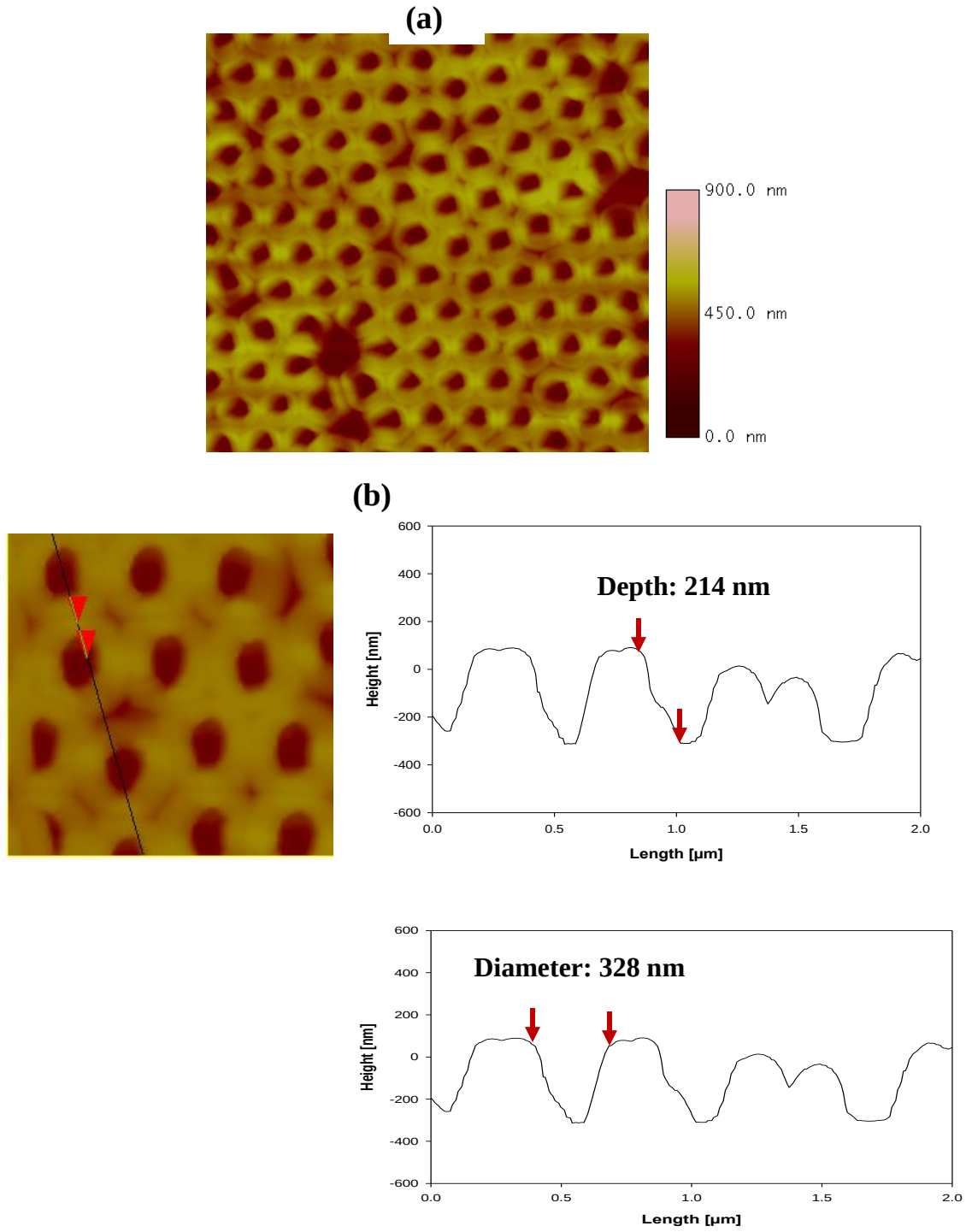


**Figure 30:** (a) A 10 µm x 10 µm AFM image of nano-wells in the titania film surface after 60 days soaking in 0.1 M KCl. (b) Section analysis show that the depths and the heights are the same as on day 1.

It was also noticed that similar CV's were obtained for films using the three redox probes indicating that there is no probe dependent effect on the stability studies. Surface characterization of films (with spheres) using AFM was done on the samples taken out on day 60 from 0.1 M KCl solution to confirm the compactness of the film. Similar AFM and SEM images as observed on day 1 were noticed on day 60 (Figure 29). At the blocked films with nano-wells, though the major part of the CV overlaps with that of the bare electrode, a small shift in the peak potential of the CV (compared to bare ITO) was observed for all the redox probes (see Figures 26, 27 and 28) from the first day till the 60$^{th}$ day. To confirm that it was not due to the changes in nano-well surface morphology, AFM images were taken on day 1 and day 60. The AFM images on day 60 showed consistent packing with similar depth and height profiles when compared with the samples from the first day of the stability studies (see Figure 30).

The hypothesis that titania films are more stable than conventional silica based sol-gel systems was evaluated by repeating the stability tests for silica films (with spheres) as previously reported by Collinson's group.[101] To prove this hypothesis, a procedure developed by Kanungo et al. for fabrication of well-packed, monolayer templated silica films was adopted.[76] Calcination of $SiO_2$ films with PS spheres cannot be used to remove the template because the silica film cracks and flakes off the surface at high temperatures (> 100$^{o}$C). Thus, the films were soaked in chloroform to remove PS template. The silica films with spheres and nano-wells were then immersed in 0.1 M KCl for 7 days. The samples were taken out of solution and CV's were collected every two days. Figure 31 (a) shows the CV's of 1 mM of $FcCH_2OH$ at the bare ITO, silica film with spheres and silica

film with nano-wells on day one. As can be noticed in Figure 31 (b), there was an increase in Faradaic current for silica films with spheres from day 1 to day 3 to day 6. Also, the shape of the CV's changed from day 1 to day 5 (peak shaped). This can be due to the $SiO_2$ film (with spheres) falling off the substrate or development of defects in $SiO_2$ matrix. In agreement with CV results, optical images and surface characterization by AFM for samples in 0.1 M KCl on day 1 [see Figure 32 (a) and 32 (c)] and day 5 [see Figure 32 (b) and 32 (d)] confirm that the reason for the increase in current was because the films were falling off the substrate. From the comparison of the stability studies between silica and titania films containing PS template, it is shown that the titania films are stable for longer period of time in aqueous solutions (water, 0.1 M KCl).

Two different explanations can be attributed to the greater stability of amorphous $TiO_2$ films when compared to amorphous $SiO_2$ films. While one explanation is based on the point of zero charge (pzc) of the oxide film, the other is based on the coordination number (CN) of the metal site in the amorphous film. Lobbus and co-workers stated that the dissolution of solid oxide materials mainly depend on the pH dependent charge state of the film. The oxides showed the least solubility in solutions that have pH around the point-of-zero charge (pzc).[112, 113] In the present study, the titania films prepared from amine-complexed sol have a pH around the pzc of titanium which is approximately 6.0. Hence, the films when placed in aqueous solutions (0.1 M KCl is neutral) with pH 6-7, close to the pzc of titanium (6.5) showed the least solubility. Whereas silica films prepared from the acid-catalysed sol (pH = 4) are positively charged. Such $SiO_2$ films when placed in neutral

solutions having pH 7, exhibit greater dissolution since the pH of the solution (pH = 7) is much greater than pzc of silica (pH = 2).

Secondly, dissolution of silica materials in aqueous solutions is enhanced by $OH^-$ ions that get chemisorbed at the tetrahedral Si site having non-bridging oxygens resulting in rearrangement into a five-coordinated intermediate. This weakens the oxygen bonds in the underlying silica surface, further breaking the Si-O-Si bonds.[2, 4, 136] On the other hand, amorphous titania has a distorted octahedral network structure with the central titanium metal having a coordination number of 6.[137] Hence when these films are placed in aqueous solutions, it is not possible for $OH^-$ ions to catalyze the dissolution process (by increasing the coordination number) as the central titanium atom has already reached its maximum coordination number.

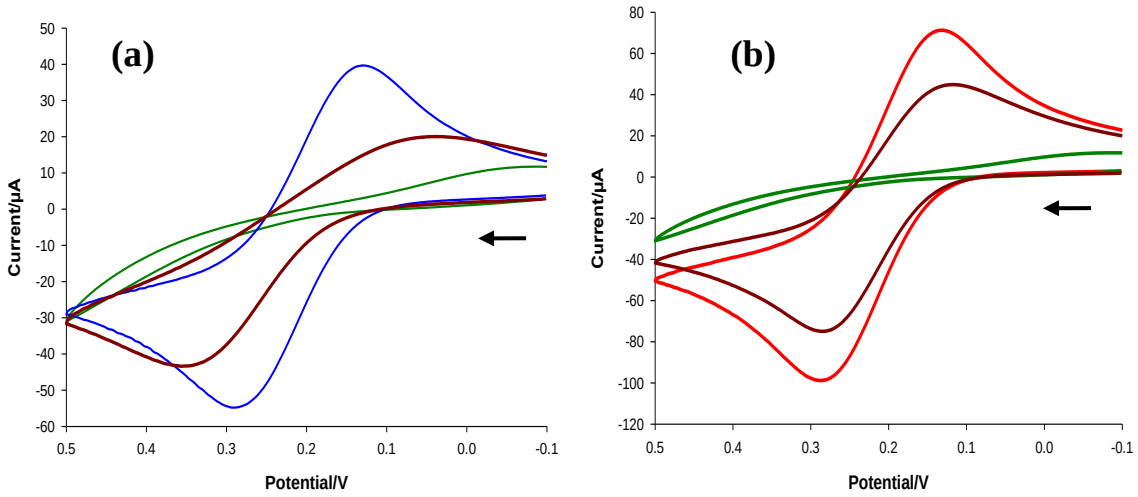


**Figure 31:** (a) CV's of 1 mM $FcCH_2OH$ in 0.1M KCl at bare electrode (red), "blocked" $SiO_2$ film with PS spheres (green), "blocked" $SiO_2$ film after template (PS) removal (brown) (b) Expansion of the CV's of 1 mM $FcCH_2OH$ in 0.1 M KCl at "blocked" $SiO_2$ films with PS spheres after soaking in 0.1 M KCl for 1 (green), 3 (brown) and 5 (blue) days.

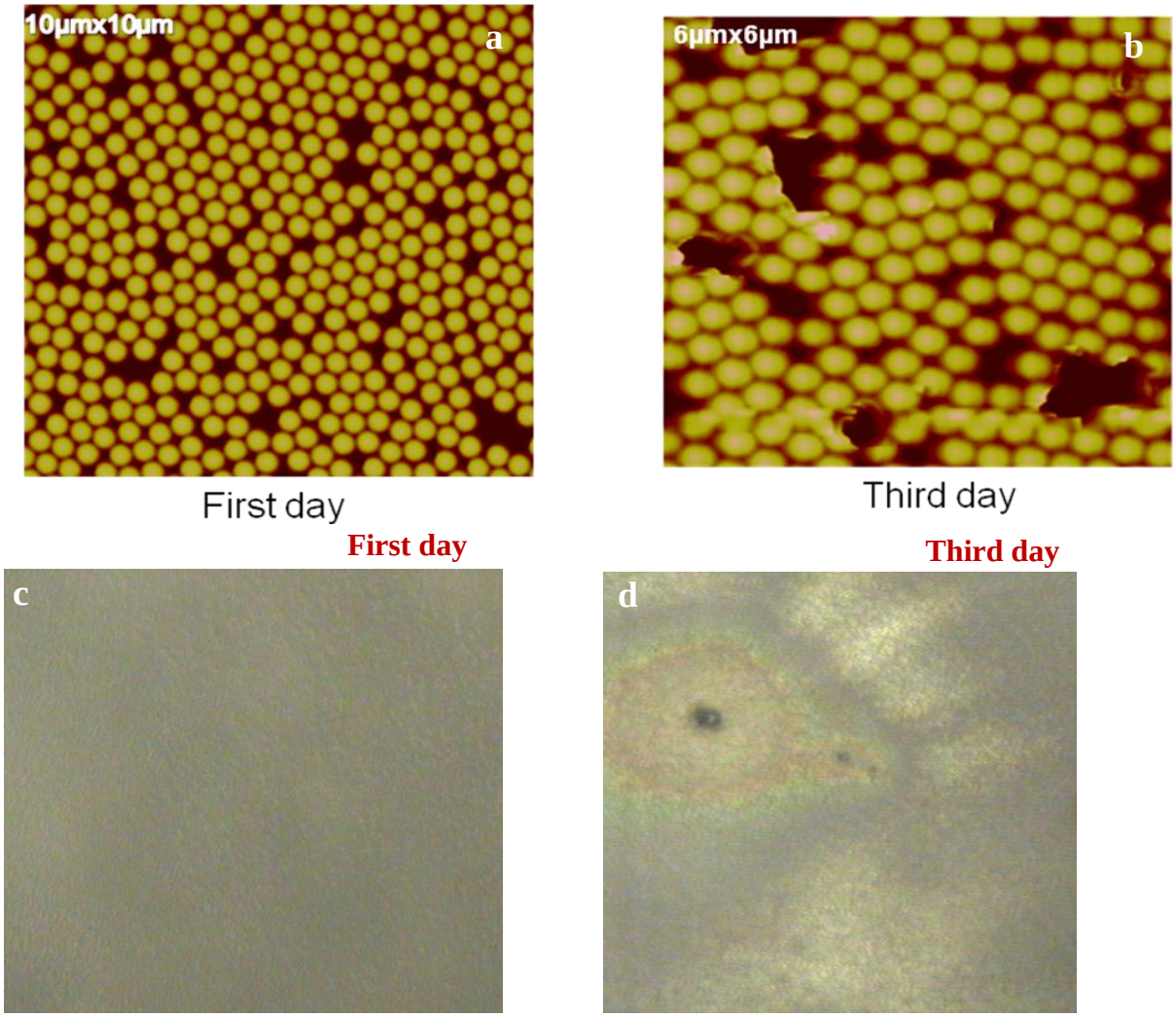


**Figure 32:** (a) A 10 µm x 10 µm AFM image of $SiO_2$ film with PS spheres before soaking in 0.1 M KCl (b) A 6 µm x 6 µm AFM image of $SiO_2$ film with PS spheres after soaking in 0.1 M KCl for 3 days. (c) Optical image of $SiO_2$ film with PS spheres before soaking in 0.1 M KCl. (d) Optical image of $SiO_2$ film with PS spheres after soaking in 0.1 M KCl for 3 days.

**3.5 Growing of nanostructures inside the templated films:** The nano-wells in titania films can be used as templates to grow nanostructures inside them. In order to prove that the bottom of the cavity is accessible for growing nanostructures, copper was electrodeposited by reducing $Cu^{+2}$ ions to Cu at a particular voltage. From the CV shown in Figure 34 (a), a reduction potential of -0.25 V for 60 sec was selected for the deposition of copper in the nanowells. The size of the copper deposited in the nano-wells will depend on potential as well as the deposition time. More negative potentials and longer deposition times should result in an increase in the amount of copper deposited. Application of negative potentials above -0.30 V resulted in over deposition of copper leading to surface contamination as shown in Figure 33. Hence, an optimal potential and deposition time needs to be selected to achieve reasonable growth. Figure 34 (b) shows the AFM image of nano-wells after electrodeposition of copper at -0.25 V. The section analysis shows that copper has been electrochemically reduced inside the nanowells and the height of copper deposited was measured to be 43.8 ± 8.2 nm (N = 10). However, the deposition of copper was not uniform thoughout the nanowells. About 60 % of the wells have copper deposition; while some have overdeposition and few are seen to have only a small deposition. To have an uniform deposition of copper in all the nano-wells, several conditions like cleaning of the nano-wells, appropriate potential and deposition time should be considered for further improvement. Also, the presence of copper in the nano-wells should be confirmed by using elemental analysis techniques like energy dispersive X-ray spectroscopy (EDS) and X-ray photoelectron spectroscopy (XPS). As shown from

this experiment, the templated titania films are accessible to grow nanostructures which can have future applications in designing "nano-electrodes" within the porous matrix.

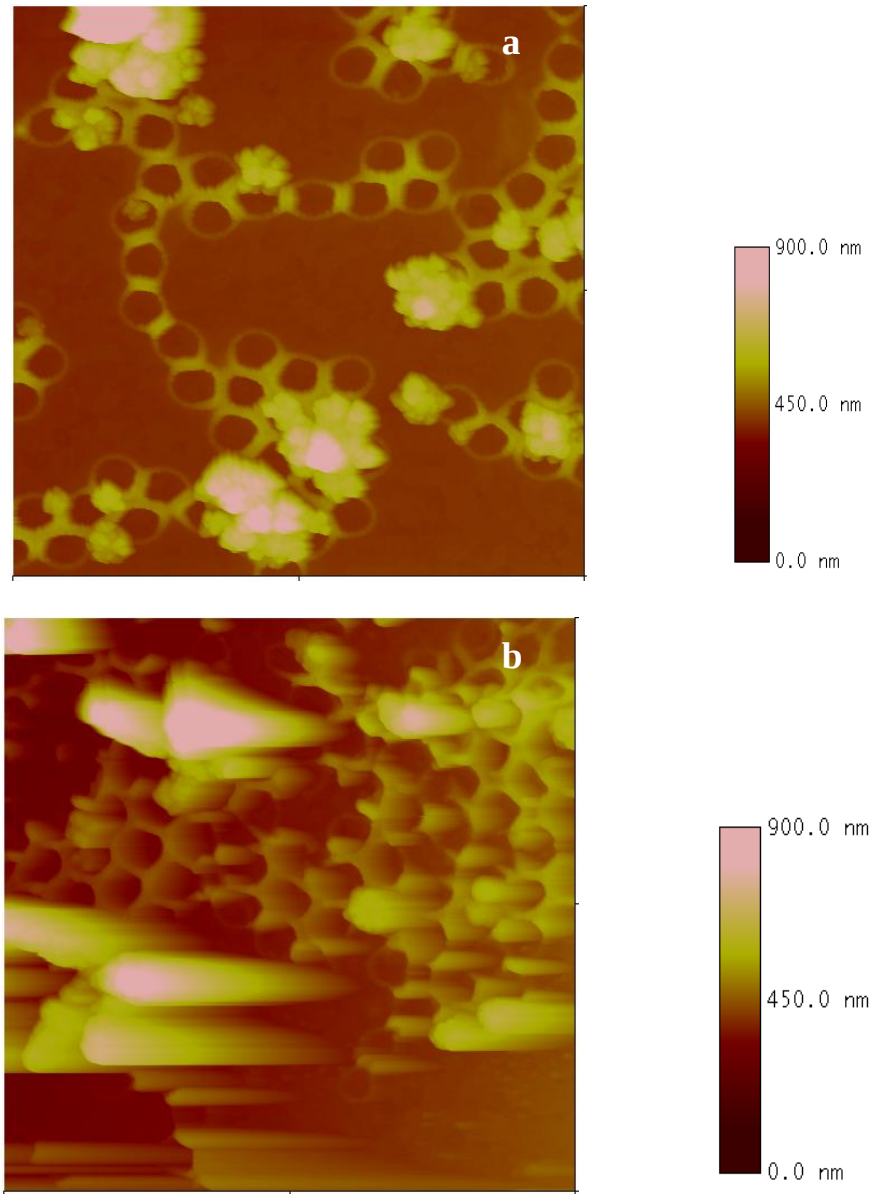


**Figure 33:** (a) A 5 µm x 5 µm AFM image of titania templated film after applying -0.35 V for 60 sec in 5 mM $CuSO_4$ in 0.1 M $H_2SO_4$. (b) A 5 µm x 5 µm AFM image of titania templated film after applying -0.4 V for 60 sec in 5 mM $CuSO_4$ in 0.1 M $H_2SO_4$. Both the AFM images show over deposition of copper in the nano-wells at more negative voltages.

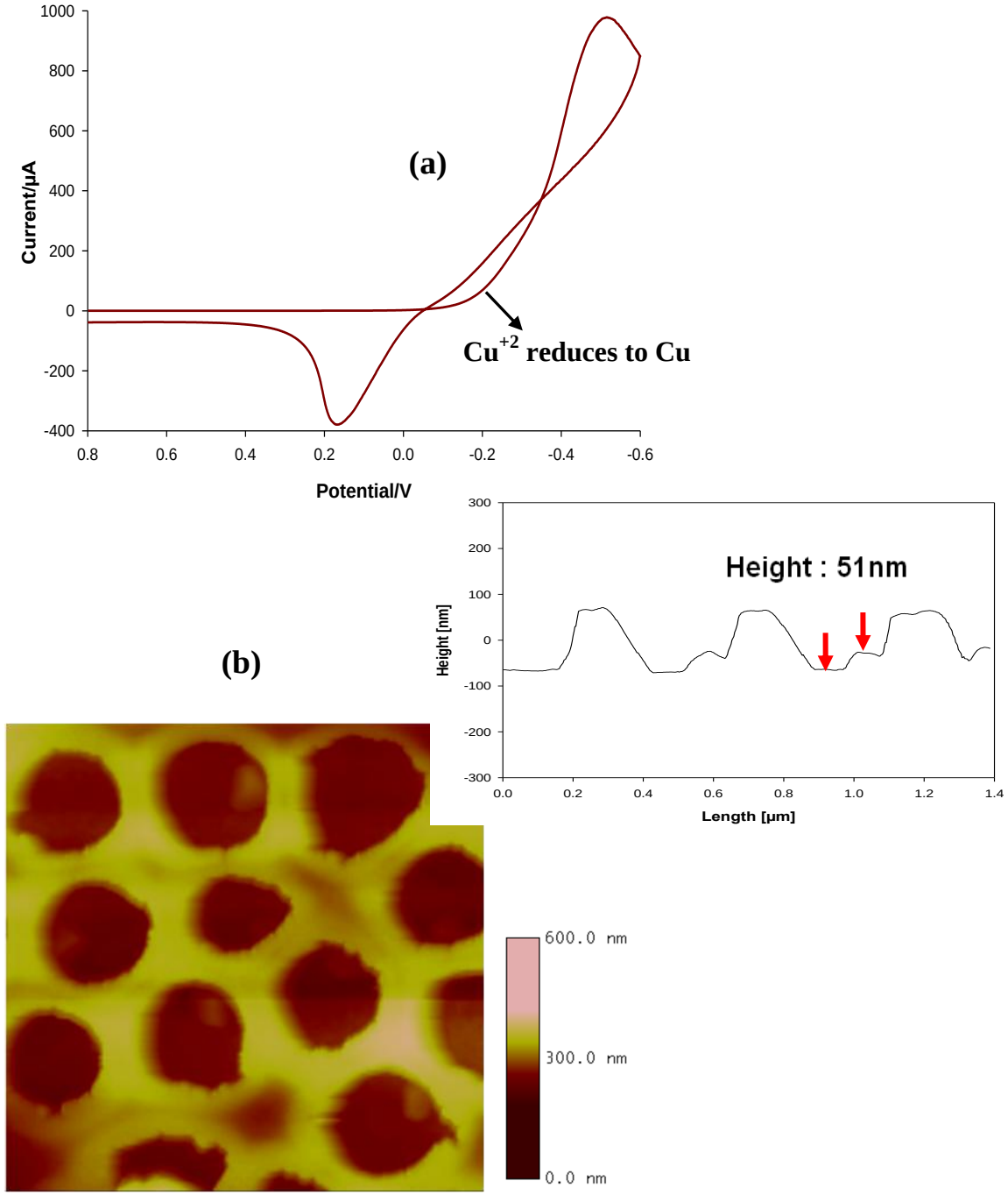


**Figure 34:** (a) CV of 5 mM $CuSO_4$ in 0.1 M $H_2SO_4$ at the "blocked" templated film. (b) A 2 µm x 2 µm AFM image of templated film after applying -0.25 V for 60 sec in 5 mM $CuSO_4$ in 0.1 M $H_2SO_4$.

# CHAPTER 4 Conclusions

Polystyrene spheres were used as templates to create 2-D close packed arrays of nano-wells inside the titania matrix. Initially, the titania sol containing PS spheres was spun on the ITO substrate. After achieving a monolayer of packed PS spheres in the $TiO_2$ matrix, the PS spheres were removed completely by calcination which forms nano-wells inside the titania films. Cyclic voltammetry was used to confirm the complete removal of PS spheres from the titania films. Cyclic voltammetry results indicate that titania films soaked in aqueous solution did not show any defects over a period of two months. Also, the surface characterization of the films doped with PS spheres and films with nano-wells using AFM and SEM support the results obtained from CV's. The surface morphology of the films in solution for 60 days looks similar to that of the films before soaking in solution. Whereas for silica, the results obtained from CV and AFM show that defects arise after 3 days in 0.1 M KCl resulting in the film falling off from the substrate surface. Hence, templated titania films were more stable in aqueous solutions compared to the conventional silica sol-gel systems which tend to fall off within a week.

With the advantage of long-term stability in aqueous solutions, the templated titania films can be used to grow nanostructures inside the nano-wells. To prove that the nano-

wells are accessible for growing nanostructures, copper was electrochemically deposited in them.

**Future directions:** Future work on this project can include determining the accessibility of the nano-wells by doing conducting-AFM. Also, electrodeposition of copper inside the nano-wells can be improved so that uniform deposition is seen in all the nano-wells. Some of the factors which can improve the electrodeposition of copper include cleaning of the nano-wells, potential applied and deposition time. Further, the deposition of copper as a function of time and potential can be studied.

Another future direction of this project could be that these nano-wells in the titania films, being open to the substrate surface, can have applications in chemical sensing.[76] In general, biomolecules such as enzymes have been immobilized in sol-gel materials, thus protecting the enzyme against extreme conditions such as high temperature, high pH and organic solvents. This stabilization enables such molecules to have application as chemical sensors in harsh environmental conditions.

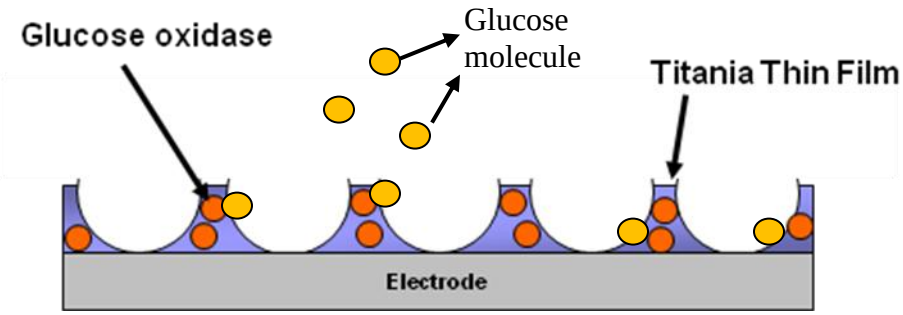


**glucose + $O_2$ + $GO_{(ox)}$ → gluconolactone +$GO_{(red)}$ + $H_2O_2$**

**Figure 35:** Example of an application of titania nano-materials in glucose sensing.

One good example for application of titania nano-materials is for measuring the blood glucose levels. The higher surface area and porosity of the templated titania materials enable the glucose molecule in solution to easily diffuse through the films to the underlying substrate surface. Also, the materials can be exposed to solutions for longer durations due to the stability of these materials in aqueous solutions. Hence this sol-gel derived $TiO_2$ biological sensor will likely have faster response times, good sensitivity and better stability. Glucose oxidase (GO) could be easily entrapped into the films and this can be used to catalyze the oxidation of glucose in the presence of oxygen to form gluconic acid and hydrogen peroxide as shown in Figure 35.[123, 127, 128] Detection of glucose is carried out using electrochemical techniques. From the amperometric response generated by the electrochemical oxidation of hydrogen peroxide at the electrode surface, the amount of glucose in the sample can be estimated.[127, 128]

## Literature Cited

Literature Cited


1. Lev, O.; Tsionsky, M.; Rabinovich, L.; Glezer, V.; Sampath, S.; Pankratov, I.; Gun, J., Organically Modified Sol-Gel Sensors. *Anal. Chem.* **1995,** *67* (1), 22A-30A.
2. Iler, R. K., *The Chemistry of Silica*. JOHN WILEY & SONS: New York, 1979.
3. Bunker, B. C., Molecular Mechanisms for Corrosion of Silica and Silicate-Glasses. *J. Non-cryst. Solids* **1994,** *179*, 300-308.
4. Wirth, G. S.; Gieskes, J. M., Initial Kinetics Of The Dissolution Of Vitreous-Silica In Aqueous-Media. *J. Colloid Interface Sci.* **1979,** *68* (3), 492-500.
5. Brinker, J.; Scherer, G., *Sol-Gel Science*. Academic Press: New York, 1990.
6. Hench, L. L.; West, J. K., THE SOL-GEL PROCESS. *Chem. Rev.* **1990,** *90* (1), 33-72.
7. Brinker, C. J.; Hurd, A. J.; Schunk, P. R.; Frye, G. C.; Ashley, C. S., Review of Sol-Gel Thin Film Formation. *J. Non-Cryst. Solids* **1992,** *147-148*, 424-436.
8. Shacham, R.; Avnir, D.; Mandler, D., Electrodeposition of Methylated Sol-Gel Films on Conducting Surfaces. *Adv. Mater.* **1999,** *11* (5), 384-388.
9. Deepa, P. N.; Kanungo, M.; Claycomb, G.; Sherwood, P. M. A.; Collinson, M. M., Electrochemically Deposited Sol-Gel-Derived Silicate Films as a Viable Alternative in Thin-Film Design. *Anal. Chem.* **2003,** *75* (20), 5399-5405.
10. Collinson, M. M.; Moore, N.; Deepa, P. N.; Kanungo, M., Electrodeposition of Porous Silicate Films from Ludox Colloidal Silica. *Langmuir* **2003,** *19* (18), 7669-7672.
11. Brinker, C. J.; Frye, G. C.; Hurd, A. J.; Ashley, C. S., Fundamentals of Sol-Gel Dip Coating. *Thin Solid Films* **1991,** *201*, 97-108.
12. Collinson, M. M., Recent trends in analytical applications of organically modified silicate materials. *TrAC, Trends Anal. Chem.* **2002,** *21* (1), 30-38.
13. Collinson, M. M., Analytical applications of organically modified silicates. *Mikrochim. Acta* **1998,** *129* (3-4), 149-165.
14. Pagliaro, M.; Ciriminna, R.; Man, M. W. C.; Campestrini, S., Better Chemistry Through Ceramics: The Physical Bases of the Outstanding Chemistry of ORMOSIL. *J. Phys. Chem. B* **2006,** *110*, 1976-1988.
15. Avnir, D.; Braun, S.; Lev, O.; Levy, D.; Ottolenghi, M., Organically Doped Sol-Gel Porous Glasses: Chemical Sensors, Enzymatic Sensors, Electrooptical Materials, Luminescent Materials and Photochromic Materials. *In Sol-Gel Optics Processing and Applications*, Klein, L. C., Ed. Kluwer Academic Publications: Massachusetts, 1994; pp 539-582.
16. Avnir, D., Organic Chemistry within Ceramic Matrices: Doped Sol-Gel Materials. *Acc. Chem. Res.* **1995,** *28*, 328-334.

17. Sanchez, S.; Ribot, F., Design of Hybrid Organic-Inorganic Materials Synthesized via Sol-Gel Chemistry. *New J. Chem.* **1994,** *18*, 1007-1047.
18. Rottman, C.; Grader, G.; Avnir, D., Polarities of Sol-Gel-Derived Ormosils and of Their Interfaces with Solvents. *Chem. Mater.* **2001,** *13*, 3631-3634.
19. Sanchez, C.; Lebeau, B.; Chaput, F.; Boilot, J.-P., Optical Properties of Functional Hybrid Organic-Inorganic Nanocomposites. *Adv. Mater.* **2003,** *15* (23), 1969-1994.
20. Blum, J.; Avnir, D.; Schumann, H., Sol-Gel Encapsulated Transition-Metal Catalysts. *Chem. tech.* **1999**, 32-38.
21. Corma, A., From Microporous to Mesoporous Molecular Sieve Materials and Their Use in Catalysis. *Chem. Rev.* **1997,** *97*, 2373-2419.
22. Collinson, M. M., *Structure, Chemistry, and Applications of Sol-Gel Derived Materials*. Academic Press: 2001; Vol. 5: Chalcogenides Glasses and Sol-gel Materials,.
23. Howells, A. R.; Zambrano, P. J.; Collinson, M. M., Diffusion of Redox Probes in Hydrated Sol-Gel-Derived Glasses. *Anal. Chem.* **2000,** *72* (21), 5265-5271.
24. Avnir, D.; Braun, S.; Lev, O.; Ottolenghi, M., Enzymes and Other Proteins Entrapped in Sol-Gel Materials. *Chem. Mater.* **1994,** *6* (10), 1605-1614.
25. Wolfbeis, O. S.; Reisfeld, R.; Oehme, I., Sol Gels and Chemical Sensors. *In Structure and Bonding*, Springer-Verlag: Berlin, 1996; Vol. 85, pp 51-98.
26. Lin, J.; Brown, C. W., Sol-gel glass as a matrix for chemical and biochemical sensing. *Trac-Trends Anal. Chem.* **1997,** *16* (4), 200-211.
27. Mackenzie, J. D., *Ultrastructure Processing of Glasses, Ceramics, and Composites*. Wiley: New York, 1984.
28. Avnir, D.; Braun, S.; Lev, O.; Ottolenghi, M., Enzymes and Other Proteins Entrapped in Sol-Gel Materials. *Chem. Mater.* **1994,** *6*, 1605-1614.
29. Lu, Y. F.; Cao, G. Z.; Kale, R. P.; Prabakar, S.; Lopez, G. P.; Brinker, C. J., Microporous silica prepared by organic templating: Relationship between the molecular template and pore structure. *Chem. Mater.* **1999,** *11* (5), 1223-1229.
30. Olson, D. A.; Chen, L.; Hillmyer, M. A., Templating nanoporous polymers with ordered block copolymers. *Chem. Mater.* **2008,** *20* (3), 869-890.
31. Behrens, P.; Stucky, G. D., Ordered Molecular Arrays as Templates - A New Approach to the Synthesis of Mesoporous Materials. *Angew. Chem.-Int. Ed. in English* **1993,** *32* (5), 696-699.
32. Wan, Y.; Shi, Y. F.; Zhao, D. Y., Designed synthesis of mesoporous solids via nonionic-surfactant-templating approach. *Chem. Commun.* **2007,** (9), 897-926.
33. Stein, A.; Schroden, R. C., Colloidal crystal templating of three-dimensionally ordered macroporous solids: materials for photonics and beyond. *Curr. Opin. Solid State Mater. Sci.* **2001,** *5* (6), 553-564.
34. Jaroniec, M.; Schuth, F., Preface to the special issue: Templated materials. *Chem. Mater.* **2008,** *20* (3), 599-600.
35. Raman, N. K.; Anderson, M. T.; Brinker, C. J., Template-based approaches to the preparation of amorphous, nanoporous silicas. *Chem. Mater.* **1996,** *8* (8), 1682-1701.
36. Fh, D., The Preparation of Specific Adsorbents. *Proc. Nat. Acad. Sci.* **1949,** *35* (5), 227-229.

37. Imhof, A.; Pine, D. J., Ordered macroporous materials by emulsion templating. *Nature* **1997,** *389* (6654), 948-951.
38. Xia, Y. N.; Gates, B.; Yin, Y. D.; Lu, Y., Monodispersed colloidal spheres: Old materials with new applications. *Adv. Mater.* **2000,** *12* (10), 693-713.
39. Wan, Y.; Zhao, D. Y., On the controllable soft-templating approach to mesoporous silicates. *Chem. Rev.* **2007,** *107* (7), 2821-2860.
40. Antonietti, M., Surfactants for novel templating applications. *Curr. Opin. Colloid Interface Sci.* **2001,** *6* (3), 244-248.
41. Palmqvist, A. E. C., Synthesis of ordered mesoporous materials using surfactant liquid crystals or micellar solutions. *Curr. Opin. Colloid Interface Sci.* **2003,** *8* (2), 145-155.
42. Hedden, R. C.; Bauer, B. J.; Smith, A. P.; Grohn, F.; Amis, E., Templating of inorganic nanoparticles by PAMAM/PEG dendrimer-star polymers. *Polymer* **2002,** *43* (20), 5473-5481.
43. Rogers, M. C.; Adisa, B.; Bruce, D. A., Synthesis and characterization of dendrimer-templated mesoporous oxidation catalysts. *Catal. Lett.* **2004,** *98* (1), 29-36.
44. Hukkamaki, J.; Pakkanen, T. T., Amorphous silica materials prepared by neutral templating route using amine-terminated templates. *Microporous Mesoporous Mater.* **2003,** *65* (2-3), 189-196.
45. Jahromi, S.; Mostert, B., Templating nanoporosity in polyorganosilicates using reactive dendrimers. *Macromolecules* **2004,** *37* (6), 2159-2162.
46. Wei, Y.; Xu, J. G.; Dong, H.; Dong, J. H.; Qiu, K. Y.; Jansen-Varnum, S. A., Preparation and physisorption characterization of D-glucose-templated mesoporous silica sol-gel materials. *Chem. Mater.* **1999,** *11* (8), 2023-2029.
47. Liu, S. T.; Wood, L. F.; Ohman, D. E.; Collinson, M. M., Creating aligned arrays of Bacillus megaterium in sol-gel matrixes. *Chem. Mater.* **2007,** *19* (11), 2752-2756.
48. Zhou, H.; Fan, T. X.; Zhang, D., Hydrothermal synthesis of ZnO hollow spheres using spherobacterium as biotemplates. *Microporous Mesoporous Mater.* **2007,** *100* (1-3), 322-327.
49. Sotiropoulou, S.; Sierra-Sastre, Y.; Mark, S. S.; Batt, C. A., Biotemplated nanostructured materials. *Chem. Mater.* **2008,** *20* (3), 821-834.
50. Cao, G. Z.; Liu, D. W., Template-based synthesis of nanorod, nanowire, and nanotube arrays. *Adv. Colloid Interface Sci.* **2008,** *136* (1-2), 45-64.
51. Yan, H. W.; Blanford, C. F.; Smyrl, W. H.; Stein, A., Preparation and structure of 3D ordered macroporous alloys by PMMA colloidal crystal templating. *Chem. Commun.* **2000,** (16), 1477-1478.
52. Miguez, H.; Meseguer, F.; Lopez, C.; Holgado, M.; Andreasen, G.; Mifsud, A.; Fornes, V., Germanium FCC structure from a colloidal crystal template. *Langmuir* **2000,** *16* (10), 4405-4408.
53. Tessier, P. M.; Velev, O. D.; Kalambur, A. T.; Rabolt, J. F.; Lenhoff, A. M.; Kaler, E. W., Assembly of gold nanostructured films templated by colloidal crystals and use in surface-enhanced Raman spectroscopy. *J. Am. Chem. Soc.* **2000,** *122* (39), 9554-9555.

54. Tessier, P.; Velev, O. D.; Kalambur, A. T.; Lenhoff, A. M.; Rabolt, J. F.; Kaler, E. W., Structured metallic films for optical and spectroscopic applications via colloidal crystal templating. *Adv. Mater.* **2001,** *13* (6), 396-400.
55. Velev, O. D.; Tessier, P. M.; Lenhoff, A. M.; Kaler, E. W., Synthesis and application of nanostructured metallic films templated by colloidal crystals. *J. Am. Chem. Soc.* **2001,** *221*, 92.
56. Yan, H. W.; Blanford, C. F.; Holland, B. T.; Parent, M.; Smyrl, W. H.; Stein, A., A chemical synthesis of periodic macroporous NiO and metallic Ni. *Adv. Mater.* **1999,** *11* (12), 1003-1006.
57. Holland, B. T.; Blanford, C. F.; Do, T.; Stein, A., Synthesis of highly ordered, three-dimensional, macroporous structures of amorphous or crystalline inorganic oxides, phosphates, and hybrid composites. *Chem. Mater.* **1999,** *11* (3), 795-805.
58. Park, S. H.; Qin, D.; Xia, Y., Crystallization of mesoscale particles over large areas. *Adv. Mater.* **1998,** *10* (13), 1028.
59. Park, S. H.; Xia, Y. N., Fabrication of three-dimensional macroporous membranes with assemblies of microspheres as templates. *Chem. Mater.* **1998,** *10* (7), 1745.
60. Park, S. H.; Xia, Y. N., Macroporous membranes with highly ordered and three-dimensionally interconnected spherical pores. *Adv. Mater.* **1998,** *10* (13), 1045.
61. Gates, B.; Yin, Y. D.; Xia, Y. N., Fabrication and characterization of porous membranes with highly ordered three-dimensional periodic structures. *Chem. Mater.* **1999,** *11* (10), 2827-2836.
62. Velev, O. D.; Jede, T. A.; Lobo, R. F.; Lenhoff, A. M., Microstructured porous silica obtained via colloidal crystal templates. *Chem. Mater.* **1998,** *10* (11), 3597-3602.
63. Velev, O. D.; Jede, T. A.; Lobo, R. F.; Lenhoff, A. M., Porous silica via colloidal crystallization. *Nature* **1997,** *389* (6650), 447-448.
64. Yan, H. W.; Blanford, C. F.; Holland, B. T.; Smyrl, W. H.; Stein, A., General synthesis of periodic macroporous solids by templated salt precipitation and chemical conversion. *Chem. Mater.* **2000,** *12* (4), 1134-1141.
65. Holland, B. T.; Blanford, C. F.; Stein, A., Synthesis of macroporous minerals with highly ordered three-dimensional arrays of spheroidal voids. *Science* **1998,** *281* (5376), 538-540.
66. Lei, Z. B.; Li, J. M.; Zhang, Y. G.; Lu, S. M., Fabrication and characterization of highly-ordered periodic macroporous barium titanate by the sol-gel method. *J. Mater. Chem.* **2000,** *10* (12), 2629-2631.
67. Perez-Ramirez, J.; Christensen, C. H.; Egeblad, K.; Groen, J. C., Hierarchical zeolites: enhanced utilisation of microporous crystals in catalysis by advances in materials design. *Chem. Soc. Rev.* **2008,** *37* (11), 2530-2542.
68. Beck, J. S.; Vartuli, J. C.; Roth, W. J.; Leonowicz, M. E.; Kresge, C. T.; Schmitt, K. D.; Chu, C. T. W.; Olson, D. H.; Sheppard, E. W.; McCullen, S. B.; Higgins, J. B.; Schlenker, J. L., A New Family of Mesoporous Molecular-Sieves Prepared with Liquid-Crystal Templates. *J. Am. Chem. Soc.* **1992,** *114* (27), 10834-10843.

69. Kresge, C. T.; Leonowicz, M. E.; Roth, W. J.; Vartuli, J. C.; Beck, J. S., Ordered Mesoporous Molecular-Sieves Synthesized by a Liquid-Crystal Template Mechanism. *Nature* **1992,** *359* (6397), 710-712.
70. Davis, M. E., Ordered porous materials for emerging applications. *Nature* **2002,** *417* (6891), 813-821.
71. Holland, B. T.; Abrams, L.; Stein, A., Dual templating of macroporous silicates with zeolitic microporous frameworks. *J. Am. Chem. Soc.* **1999,** *121* (17), 4308-4309.
72. Yin, J. S.; Wang, Z. L., Plasmon energy shift in mesoporous and double length-scale ordered nanoporous silica. *Appl. Phys. Lett.* **1999,** *74* (18), 2629-2631.
73. Luo, Q.; Li, L.; Yang, B.; Zhao, D. Y., Three-dimensional ordered macroporous structures with mesoporous silica walls. *Chem. Lett.* **2000,** (4), 378-379.
74. Wu, X. F.; Tian, Y. J.; Cui, Y. B.; Wei, L. Q.; Wang, Q.; Chen, Y. F., Raspberry-like silica hollow spheres: Hierarchical structures by dual latex-surfactant templating route. *J. Phys. Chem. C* **2007,** *111* (27), 9704-9708.
75. Lu, Y. F.; Ganguli, R.; Drewien, C. A.; Anderson, M. T.; Brinker, C. J.; Gong, W. L.; Guo, Y. X.; Soyez, H.; Dunn, B.; Huang, M. H.; Zink, J. I., Continuous formation of supported cubic and hexagonal mesoporous films by sol gel dip-coating. *Nature* **1997,** *389* (6649), 364-368.
76. Kanungo, M.; Deepa, P. N.; Collinson, M. M., Template-directed formation of hemispherical cavities of varying depth and diameter in a silicate matrix prepared by the sol-gel process. *Chem. Mater.* **2004,** *16* (25), 5535-5541.
77. Khramov, A. N.; Munos, J.; Collinson, M. M., Preparation and characterization of macroporous silicate films. *Langmuir* **2001,** *17* (26), 8112-8117.
78. Brisson, V.; Tilton, R. D., Self-assembly and two-dimensional patterning of cell arrays by electrophoretic deposition. *Biotechnol. and Bioeng.* **2002,** *77* (3), 290-295.
79. Xia, Y.; Gates, B.; Yin, Y.; Lu, Y., Monodispersed Colloidal Spheres: Old Materials with New Applications. *Adv. Mater.* **2000,** *12* (10), 693-713.
80. McComb, D. W.; Treble, B. M.; Smith, C. J.; De La Rue, R. M.; Johnson, N. P. In Synthesis and characterisation of photonic crystals, **2001**;142-148.
81. Wijnhoven, J.; Zevenhuizen, S. J. M.; Hendriks, M. A.; Vanmaekelbergh, D.; Kelly, J. J.; Vos, W. L., Electrochemical assembly of ordered macropores in gold. *Adv. Mater.* **2000,** *12* (12), 888-890.
82. Braun, P. V.; Wiltzius, P., Microporous materials - Electrochemically grown photonic crystals. *Nature* **1999,** *402* (6762), 603-604.
83. Braun, P.; Wiltzius, P., Electrochemical fabrication of 3D microperiodic porous materials. *Adv. Mater.* **2001,** *13* (7), 482.
84. Muller, M.; Zentel, R.; Maka, T.; Romanov, S. G.; Torres, C. M. S., Photonic crystal films with high refractive index contrast. *Adv. Mater.* **2000,** *12* (20), 1499-1503.
85. Zakhidov, A. A.; Baughman, R. H.; Iqbal, Z.; Cui, C. X.; Khayrullin, I.; Dantas, S. O.; Marti, I.; Ralchenko, V. G., Carbon structures with three-dimensional periodicity at optical wavelengths. *Science* **1998,** *282* (5390), 897-901.
86. Jiang, P.; Cizeron, J.; Bertone, J. F.; Colvin, V. L., Preparation of macroporous metal films from colloidal crystals. *J. Am. Chem. Soc.* **1999,** *121* (34), 7957-7958.

87. Wang, D. Y.; Caruso, F., Fabrication of polyaniline inverse opals via templating ordered colloidal assemblies. *Adv. Mater.* **2001,** *13* (5), 350-353.
88. Luo, G.; Liu, Z. J.; Li, L.; Xie, S. H.; Kong, J. L.; Zhao, D. Y., Creating highly ordered metal, alloy, and semiconductor macrostructures by electrodeposition, ion spraying, and laser spraying. *Adv. Mater.* **2001,** *13* (4), 286.
89. Matsushita, S.; Miwa, T.; Fujishima, A., Preparation of a new nanostructured $TiO_2$ surface using a two-dimensional array-based template. *Chem. Lett.* **1997,** (9), 925-926.
90. Egan, G. L.; Yu, J. S.; Kim, C. H.; Lee, S. J.; Schaak, R. E.; Mallouk, T. E., Nanoscale metal replicas of colloidal crystals. *Adv. Mater.* **2000,** *12* (14), 1040-1042.
91. Yang, P. D.; Rizvi, A. H.; Messer, B.; Chmelka, B. F.; Whitesides, G. M.; Stucky, G. D., Patterning porous oxides within microchannel networks. *Adv. Mater.* **2001,** *13* (6), 427-431.
92. Johnson, S. A.; Ollivier, P. J.; Mallouk, T. E., Ordered Mesoporous Polymers of Tunable Pore Size from Colloidal Silica Templates. *Science* **1999,** *283*, 963-965.
93. Xu, L. B.; Zhou, W. L.; Kozlov, M. E.; Khayrullin, II; Udod, I.; Zakhidov, A. A.; Baughman, R. H.; Wiley, J. B., Metal sphere photonic crystals by nanomolding. *J. Am. Chem. Soc.* **2001,** *123* (4), 763-764.
94. Jiang, P.; Bertone, J. F.; Colvin, V. L., A lost-wax approach to monodisperse colloids and their crystals. *Science* **2001,** *291* (5503), 453-457.
95. Khramov, A. N.; Collinson, M. M., Sol-gel preparation of macroporous silica films by templating with polystyrene microspheres. *Chem. Commun.* **2001,** (8), 767-768.
96. Levy, D.; Gigozin, I.; Zamir, I.; Kuyavskaya, B. I.; Ottolenghi, M.; Avnir, D.; Lev, O., Immobilization of Quaternary Ammonium Anion-Exchangers in Sol-Gel Glasses. *Separation Sci. Technol.* **1992,** *27* (5), 589-597.
97. Tian, S. J.; Wang, J. J.; Jonas, U.; Knoll, W., Inverse opals of polyaniline and its copolymers prepared by electrochemical techniques. *Chem Mater.* **2005,** *17* (23), 5726-5730.
98. Song, Y. Y.; Zhang, D.; Gao, W.; Xia, X. H., Nonenzymatic glucose detection by using a three-dimensionally ordered, macroporous platinum template. *Chemistry-a European Journal* **2005,** *11* (7), 2177-2182.
99. Delange, R. S. A.; Hekkink, J. H. A.; Keizer, K.; Burggraaf, A. J., Polymeric-Silica-Based Sols for Membrane Modification Applications - Sol-Gel Synthesis and Characterization with SAXS. *J. Non-Cryst. Solids* **1995,** *191* (1-2), 1-16.
100. Dunphy, D. R.; Singer, S.; Cook, A. W.; Smarsly, B.; Doshi, D. A.; Brinker, C. J., Aqueous stability of mesoporous silica films doped or grafted with aluminum oxide. *Langmuir* **2003,** *19* (24), 10403-10408.
101. Collinson, M. M.; Wang, H. M.; Makote, R.; Khramov, A., The effects of drying time and relative humidity on the stability of sol-gel derived silicate films in solution. *J. Electroanal. Chem.* **2002,** *519* (1-2), 65-71.
102. Shen, S. C.; Kawi, S., Understanding of the effect of Al substitution on the hydrothermal stability of MCM-41. *J. Phys. Chem. B* **1999,** *103* (42), 8870-8876.

103. Shen, S. C.; Kawi, S., MCM-41 with improved hydrothermal stability: Formation and prevention of Al content dependent structural defects. *Langmuir* **2002,** *18* (12), 4720-4728.
104. Mokaya, R., Template-directed stepwise post-synthesis alumination of MCM-41 mesoporous silica. *Chem. Commun.* **2000,** (16), 1541-1542.
105. Zhang, Z. T.; Han, Y.; Xiao, F. S.; Qiu, S. L.; Zhu, L.; Wang, R. W.; Yu, Y.; Zhang, Z.; Zou, B. S.; Wang, Y. Q.; Sun, H. P.; Zhao, D. Y.; Wei, Y., Mesoporous aluminosilicates with ordered hexagonal structure, strong acidity, and extraordinary hydrothermal stability at high temperatures. *J. Am. Chem. Soc.* **2001,** *123* (21), 5014-5021.
106. Zhang, Z.; Han, Y.; Zhu, L.; Wang, R.; Yu, Y.; Qiu, S.; Zhao, D.; Xiao, F. S., Strongly acidic and high-temperature hydrothermally stable mesoporous aluminosilicates with ordered hexagonal structure. *Angew. Chem.-Int. Ed.* **2002,** *41* (13), 2226-2226.
107. Chen, L. Y.; Jaenicke, S.; Chuah, G. K., Thermal and hydrothermal stability of framework-substituted MCM-41 mesoporous materials. *Microporous Mater.* **1997,** *12* (4-6), 323-330.
108. Chen, L. Y.; Chuah, G. K.; Jaenicke, S., Ti-containing MCM-41 catalysts for liquid phase oxidation of cyclohexene with aqueous $H_2O_2$ and tert-butyl hydroperoxide. *Catal. Lett.* **1998,** *50* (1-2), 107-114.
109. He, N. Y.; Lu, Z. H.; Yuan, C. W.; Hong, J. M.; Yang, C.; Bao, S. L.; Xu, Q. H., Effect of trivalent elements on the thermal and hydrothermal stability of MCM-41 mesoporous molecular materials. *Supramol. Sci.* **1998,** *5* (5-6), 553-558.
110. Lobmann, P., Soluble powders as precursors for TiO2 thin films. *J.Sol-Gel Sci. Technol.* **2005,** *33* (3), 275-282.
111. Rubia F. S. Lenza, W. L. V., Synthesis of Titania-Silica Materials by Sol-Gel. *Mater. Res.* **2002,** *5* (4), 497-502.
112. Schmidt, J.; Vogelsberger, W., Aqueous Long-Term Solubility of Titania Nanoparticles and Titanium(IV) Hydrolysis in a Sodium Chloride System Studied by Adsorptive Stripping Voltammetry. *J. Solution Chem.* **2009,** *38* (10), 1267-1282.
113. Lobbus, M.; Vogelsberger, W.; Sonnefeld, J.; Seidel, A., Current considerations for the dissolution kinetics of solid oxides with silica. *Langmuir* **1998,** *14* (16), 4386-4396.
114. Livage, J.; Henry, M.; Sanchez, C., Sol-Gel Chemistry Of Transition-Metal Oxides. *Prog. Solid State Chem.* **1988,** *18* (4), 259-341.
115. Yang, P. D.; Zhao, D. Y.; Margolese, D. I.; Chmelka, B. F.; Stucky, G. D., Generalized syntheses of large-pore mesoporous metal oxides with semicrystalline frameworks. *Nature* **1998,** *396* (6707), 152-155.
116. Livage, J.; Sanchez, C.; Babonneau, F., *Molecular Precursor Routes to Inorganic Solids*. Wiley-VCH: New York, **1988**; p 389-446.
117. Zhang, Y. F.; Zhang, Z. G.; Fang, X. M., Synthesis of one-dimensional $TiO_2$ nanomaterials and their nanostructures. *Prog. Chem.* **2007,** *19* (4), 494-501.
118. Chen, X. B.; Mao, S. S., Synthesis of titanium dioxide ($TiO_2$) nanomaterials. *J. Nanosci. Nanotechnol.* **2006,** *6* (4), 906-925.

119. Cao, Y. L.; Wang, Y. P.; Zhu, Y. Z.; Chen, H. B.; Li, Z. H.; Ding, J.; Chi, Y. B., Fabrication of anatase titania inverse opal films using polystyrene templates. *Superlattices Microstruct.* **2006,** *40* (3), 155-160.
120. Wijnhoven, J. E. G. J.; Bechger, L.; Vos, W. L., Fabrication and Characterization of Large Macroporous Photonic Crystals in Titania. *Chem. Mater.* **2001,** *13*, 4486-4499.
121. Li, Y. Z.; Kunitake, T.; Fujikawa, S., Efficient fabrication of large, robust films of 3D-ordered polystyrene latex. *Colloids and Surfaces a-Physicochemical and Engineering Aspects* **2006,** *275* (1-3), 209-217.
122. Rottman, C.; Ottolenghi, M.; Zusman, R.; Lev, O.; Smith, M.; Gong, G.; Kagan, M. L.; Avnir, D., Doped Sol-Gel Glasses as pH Sensors. *Mater. Lett.* **1992,** *13*, 293-298.
123. Kunzelmann, U.; Bottcher, H., Biosensor Properties of Glucose Oxidase Immobilized Within $SiO_2$ Gels. *Sensors and Actuators B* **1997,** *38-39*, 222-228.
124. Rottman, C.; Turniansky, A.; Avnir, D., Sol-gel physical and covalent entrapment of three methyl red indicators: a comparative study. *J. Sol-Gel Sci. Technol.* **1998,** *13* (1-3), 17-25.
125. Gelman, F.; Avnir, D.; Schumann, H.; Blum, J., Sol-Gel Entrapped Chiral Rhodium and Ruthenium Complexes as Recyclable Catalysts for the Hydrogenation of Itaconic Acid. *J. Mol. Catal. A.* **1999,** *146*, 123-128.
126. Audebert, P.; Demaille, C.; Sanchez, C., Electrochemical Probing of the Activity of Glucose Oxidase Embedded Sol-Gel Matrices. *Chem. Mater.* **1993,** *5*, 911-913.
127. Narang, U.; Prasad, P. N.; Bright, F. V.; Ramanathan, K.; Kumar, N. D.; Malhotra, B. D.; Kamalasanan, M. N.; Chandra, S., Glucose Biosensor Based on a Sol-Gel-Derived Platform. *Anal. Chem.* **1994,** *66*, 3139-3144.
128. Wang, B.; Li, B.; Deng, Q.; Dong, S., Amperometric Glucose Biosensor Based on Sol-Gel Organic-Inorganic Hybrid Material. *Anal. Chem.* **1998,** *70*, 3170-3174.
129. Kanungo, M.; Collinson, M. M., Fabrication of two-dimensionally ordered macroporous silica materials with controllable dimensions. *Chem. Commun. (Cambridge, United Kingdom)* **2004,** (5), 548-549.
130. Yoshida, M.; Prasad, P. N., Sol-gel-proceseed $SiO_2$/$TiO_2$/poly (vinylpyrrolidone) composite materials for optical waveguides. *Chem. Mater.* **1996,** *8* (1), 235-241.
131. Wessels, K.; Maekawa, M.; Rathousky, J.; Yoshida, T.; Wark, M.; Oekermann, T., Highly porous $TiO_2$ films from anodically deposited titanate hybrids and their photoelectrochemical and photocatalytic activity. *Microporous Mesoporous Mater.* **2008,** *111* (1-3), 55-61.
132. Su, C.; Hong, B. Y.; Tseng, C. M. In Sol-gel preparation and photocatalysis of titanium dioxide, **2004**; 119-126.
133. Bard, A. J.; Faulkner, L. R., *Electrochemical Methods: Fundamentals and Applications*. John Wiley and Sons, Inc.: New York, **1980**; p 718.
134. Wightman, R. M.; Wipf, D. O., *Voltammetry at Ultramicroelectrodes*. Marcel Dekker, Inc.: New York, **1989**; Vol. 15, p 267-353.
135. Peter T. Kissinger, W. R. H., *Laboratory techniques in electroanalytical chemistry*. second ed.; **1996**.

136. Bunker, B. C. In Molecular Mechanisms for Corrosion of Silica and Silicate-Glasses, *J. Non-cryst. Solids* **1994,** *179*, 300-308.
137. Hoang, V. V., Structural properties of simulated liquid and amorphous $TiO_2$. *Physica Status Solidi B-Basic Solid State Phys.* **2007,** *244* (4), 1280-1287.